

	of the same type this should be the numerical indicator. i.e. "1" for Video 1, "2" for Video 2, etc.	when it is uploaded to our system, and should include the file extension. i.e.: <i>Smith_Supplementary Video 1.mov</i>	Caption Describe the contents of the file
Supplementary Data	Supplementary Data	SUPPLEMENTARY_DATA_ALL.xlsx	Supplementary Data Tables 1-5

4

5 **Title: The consequences of craniofacial integration on the adaptive**
6 **radiations of Darwin's Finches and Hawaiian Honeycreepers**

7 **Guillermo Navalón^{1,2,3*}, Jesús Marugán-Lobón^{2,4}, Jen A. Bright^{5,6}, Christopher R. Cooney⁷ &**
8 **Emily J. Rayfield^{1,*}**

9 1. School of Earth Sciences, University of Bristol, Life Sciences Building, Bristol, UK

10 2. Unidad de Paleontología, Departamento de Biología, Universidad Autónoma de Madrid, Madrid, Spain

11 3. Department of Earth Sciences, University of Oxford, Oxford OX1 3AN, United Kingdom.

12 4. Dinosaur Institute, Natural History Museum of Los Angeles County, Los Angeles, CA, USA.

13 5. School of Geosciences, University of South Florida, Tampa, FL 33620, USA

14 6. Department of Biological and Marine Sciences, University of Hull, Hull HU6 7RX, UK.7.Department of Animal and Plant
15 Sciences, University of Sheffield, Sheffield S10 2TN, UK.

16 *Corresponding authors. E-mails: gn13871@bristol.ac.uk, e.rayfield@bristol.ac.uk

17

18 **The diversification of Darwin's finches and Hawaiian honeycreepers are two textbook**
19 **examples of adaptive radiation in birds. Why these two bird groups radiated while the**
20 **remaining endemic birds in these two archipelagos exhibit relatively low diversity and**
21 **disparity remains unexplained. Ecological factors have failed to provide a convincing**
22 **answer to this phenomenon, and some intrinsic causes connected to craniofacial**
23 **evolution have been hypothesized. Tight coevolution of the beak and the remainder of**
24 **the skull in diurnal raptors and parrots suggests that integration may be the prevalent**
25 **condition in landbirds (Inopinaves). This is in contrast with the archetypal relationship**
26 **between beak shape and ecology in Darwin's finches and Hawaiian honeycreepers,**
27 **which suggests the beak can adapt as a distinct module in these birds. Modularity has**
28 **therefore been proposed to underpin the adaptive radiation of these birds, allowing the**
29 **beak to evolve more rapidly and 'freely' in response to ecological opportunity. Here,**
30 **using geometric morphometrics and phylogenetic comparative methods in a broad**
31 **sample of skulls of landbirds, we show that craniofacial evolution in Darwin's finches**
32 **and Hawaiian honeycreepers appears to be characterized by a tighter coevolution of the**
33 **beak and the rest of the skull (cranial integration) than in most landbird lineages, with**
34 **rapid and extreme morphological evolution of both skull regions along constrained**
35 **directions of phenotypic space. These patterns are unique among landbirds, including**
36 **other sympatric island radiations, and therefore counter previous hypotheses by**

37 **showing that tighter cranial integration, not only modularity, can facilitate evolution**
38 **along adaptive directions.**

39 Why some lineages diversify more or less than others is a central topic in evolutionary
40 biology. Among birds, the adaptive island radiations of Darwin's finches and Hawaiian
41 honeycreepers are notable for their rapid and disparate evolution^{1,2}. These clades quickly
42 evolved to become taxonomically and morphologically more diverse than other avian
43 lineages that colonized the same oceanic archipelagos³⁻⁷. Since these phenomena were first
44 recognized^{8,9}, many different causal hypotheses have been proposed to explain such rapid
45 island radiations. Extrinsic causes, such as differences in colonization age, have been largely
46 dismissed because other slower evolving lineages of birds colonized the archipelagos at
47 similar times^{3-5,10}. Alternatively, intrinsic explanations may offer more insight^{4,5,11,12}. *In silico*
48 simulations and empirical studies show that the covariation structure of sets of characters
49 (produced by genetic, developmental, functional, or evolutionary causes) have important
50 influences in phenotypic evolution (Fig.1) (e.g.,¹³⁻¹⁵). For example, simulations show that if
51 an anatomical structure is integrated (its component parts co-evolve, *sensu*¹⁶), its phenotypic
52 evolution will be constrained along specific lines within trait space. Modularity (weaker
53 integration between component parts), in turn, allows a less constrained exploration of trait
54 space^{13,17}(Fig. 1a). Therefore, a more modular organization is traditionally believed to
55 facilitate, or even to be a precondition¹⁸ for evolvability¹⁹ by allowing component parts to
56 evolve and adapt more independently from each other^{20,21}. An alternative view is that
57 integration may enhance evolvability, by providing an adaptive line of least resistance, along
58 which species may rapidly evolve, albeit within a constrained region of trait space^{13,17,22-24}
59 (Fig. 1c). Although the degree to which integration and modularity affect evolution seems to
60 be controlled by selection, some empirical discrepancies still exist^{13,17,22-24}. It might be
61 expected that birds, a speciose vertebrate group with extremely divergent beak shapes,
62 demonstrate little covariation between the beak and the remainder of the skull. At a broad
63 macroevolutionary level this holds true and the beak evolved as a semi-independent structure
64 displaying weak integration with the rest of the skull, arguably explaining its evolutionary
65 plasticity²⁵. Yet, when integration is quantified at the family/subfamily level, studies have
66 shown strong integration between the beak and skull morphology in diurnal raptors and
67 parrots^{11,26}. Raptors and parrots occupy key phylogenetic positions at the base and within the
68 landbird (Inopinaves) radiation, respectively²⁷⁻²⁹(which also includes Darwin's finches and
69 Hawaiian honeycreepers) suggesting that strong cranial integration might be ancestral to and
70 prevalent in landbirds^{11,26}. While there is no inherent reason to preclude that selection on the
71 shape of the beak would not also lead to adaptive changes in the shape of cranium, strong
72 cranial integration within these clades has been suggested to reflect pleiotropic interactions
73 among cranial regions hampering a fine adaptation of beak shape to feeding ecology^{11,26}. This
74 is in contrast to the paradigmatic relationship between feeding ecology and beak size and
75 shape evolution in Darwin's finches^{30,31} and Hawaiian honeycreepers^{5,32} which suggests the
76 beak in these clades is able to respond effectively and more or less independently to feeding
77 selective pressures in their island ecosystems (an observation that was crucial to developing
78 the theory of natural selection^{8,33}). A key question therefore is whether relaxation of cranial
79 integration represents an evolutionary innovation in these landbird clades whereby the beak is

80 able to evolve more ‘freely’, thereby facilitating rapid evolutionary radiation^{11,12}, or if
81 integration facilitates rapid evolution along constrained adaptive directions. The recent surge
82 of interest in the implications of integration and modularity for evolvability in evolutionary
83 theory^{11,13,15,25,34} makes testing these ideas in an iconic example of adaptive radiation
84 particularly relevant. Therefore, using geometric morphometrics and phylogenetic
85 comparative methods we here quantify whether relaxed integration (modularity) between the
86 beak and skull is linked to rapid and disparate evolutionary radiation in landbirds as per
87 classic interpretations, or whether tighter integration may be key to rapid and large
88 evolutionary change.

89

90 **Results & Discussion**

91 We found that each of the major clades of landbirds diverged to unique cranial
92 morphologies (Fig. 2, Extended Data. Figs. 3-5). Parrots (Psittaciformes) are characterised by
93 a single ancestral shift towards very high rates of skull shape evolution, resulting in a
94 characteristic cranial anatomy with short, curved beaks and expanded braincases (Fig. 2).
95 Conversely, hoopoes and hornbills (Bucerotiformes) and toucans (Ramphastidae, Piciformes)
96 show similar skull shapes to parrots but have higher aspect ratio, less curved beaks (Extended
97 Data. Figs. 3-5). While passerines (Passeriformes) have radiated to explore a large proportion
98 of landbird morphological variation, they have not achieved the levels of morphological
99 variation seen in non-passerines (Fig. 2). Although most passerines display similar skull
100 morphologies and there is a slowdown in rates of skull shape evolution in the branch leading
101 to the songbirds (Passeri), a few songbird lineages diverge substantially to explore
102 morphologies approaching those of parrots or hoopoes (Fig. 2, Extended Data. 3-5). Darwin’s
103 finches and Hawaiian honeycreepers show the highest rates of beak and skull shape evolution
104 in our sample, and experienced multiple positive rate shifts within each clade. This result is
105 similar to that of other recent studies^{2,25}, suggesting that the rapidity of evolution in these
106 species is not simply a result of their relatively recent divergence relative to the other species
107 in our data. These birds also show considerable craniofacial shape disparity, including some
108 of the most extreme shapes within Passeriformes (Fig. 2).

109 We found that the beak and the skull are integrated to an extent in all landbird clades
110 (Fig. 3a, Fig. 4a). When considered as separate groups, Passeriformes have more integrated
111 skulls than non-passerines (Fig. 4a, Table 1). This is driven by high integration in the
112 songbirds (Passeri), moderately high integration in the suboscine passerines (Tyranni) within
113 the Passeriformes, and high integration in the parrots (Psittaciformes) within the non-
114 passerines (Fig. 3a, Fig. 4a, Table 1, Extended Data Fig. 10). All other clades show lower and
115 similar levels of cranial integration (Fig. 3a, 4a; Table 1). Within songbirds (Fig. 4b),
116 Passerida, the clade containing Darwin’s finches and Hawaiian honeycreepers, exhibits
117 higher levels of integration than all other passerine clades and this likely underscores the high
118 integration displayed by songbirds as a whole group. Interestingly, the Muscicapida, the other
119 passerine clade that radiated in Galapagos and Hawaii (but to a lesser extent than Darwin’s
120 finches and Hawaiian honeycreepers), display the lowest levels of integration in our sample
121 (Fig. 3b, 4b, Table 1). High levels of integration and the same pattern of covariation persist in
122 Passerida even when Darwin’s finches and Hawaiian honeycreepers are removed from the

123 analysis (Fig. 3b, 4b; for congruence of these results with other analytical conditions see SI.
124 Figs. 5 & 6, Extended Data Fig. 10, Supplementary Data 1 & 2), suggesting that craniofacial
125 covariation in these clades matches the general covariation pattern of Passerida, indicating
126 high cranial integration may be more widespread in this clade. Therefore, contrary to
127 previous suggestions, our results show that cranial evolution in the classic adaptive radiations
128 of Darwin's finches and Hawaiian honeycreepers was most likely characterised by a pattern
129 of strong integration between of the beak with the rest of the skull.

130 Although there is not a common relationship between the strength of cranial
131 integration and rates of morphological evolution for all landbirds in our data (Extended Data
132 Fig. 8), this matches expectations as recent *in silico* models and empirical data show that this
133 relationship is also critically dependent on selection impinging upon functional and
134 developmental factors^{15,17,23,24,35}. Specifically, evolution along phenotypic lines of least
135 resistance²³ predicts that, by affecting several traits in unison, higher trait covariation can
136 increase evolutionary rates if selection favours evolutionary change along the line of
137 maximum covariation^{17,23,24}, allowing more extreme morphologies to be explored^{13,36}.
138 Therefore, lack of correlation in an older lineage such as parrots (~ 30 MY crown-group
139 Psittaciformes,²⁹) may be due to clade age: this lineage has been affected by multidirectional
140 selective pressures during its long evolution, complicating the identification of a
141 straightforward relationship between strong evolutionary integration of the skull and
142 phenotypic evolution (i.e., the 'fly in a tube' model¹⁵). Conversely, Darwin's finches and
143 Hawaiian honeycreepers (and sympatric contemporaneous radiations) are much younger
144 clades (Fig. 4c), and geographically restricted to their islands, and therefore represent a rare
145 opportunity to make more detailed inferences of phenotypic evolution. Relaxed selection in
146 island ecosystems is often invoked as resulting from the availability of empty niche space and
147 scarcity of predators, particularly in newly colonized islands (i.e. 'the island rule'^{37,38}).
148 Although this selection regime is often linked to divergent evolution³⁷, it may also facilitate
149 evolution along lines of least resistance by raising the probability of selection favouring
150 change along adaptive phenotypic pathways. Although adaptive peaks could potentially arise
151 in more areas of trait space if selection is more flexible (therefore allowing more directions of
152 evolution), the most likely change will by definition be the one using the line of least
153 resistance (Fig. 1). For example, evolution along an allometric line of least resistance rather
154 than divergent evolution may have facilitated the repeated evolution of phyletic dwarfism in
155 island elephants³⁹. In a similar way, the constrained evolution of extreme morphologies
156 along the maximum covariation line in Darwin's finches and Hawaiian honeycreepers might
157 have favoured both rapid allopatric speciation and rapid niche separation by character
158 displacement within each of the families because selection facilitating change in one cranial
159 trait affected a cascade of other cranial regions³⁷. This, in turn, might underlie the
160 comparatively higher rates of morphological evolution for the whole skull, and for both the
161 beak and skull individually (Fig. 2 & SI. Tables 1-3; and see also^{2,25}). In agreement with this
162 model, we show that at the family level (or sub-family for Darwin's finches and Hawaiian
163 honeycreepers), Darwin's finches and Hawaiian honeycreepers exhibit some of the most
164 extreme shape differences along the axis of maximum covariation between the beak and the
165 skull shapes (the purported phenotypic line of least resistance; see Methods) for the

166 passeroid songbirds (Passerida) (Extended Data. Fig. 7) and for all songbirds (Fig 4c). This
167 coordinated phenotypic evolution (Extended Data. Fig. 6) might also be biomechanically
168 significant, as the jaw adductor muscles attach exclusively to the braincase block, yet act to
169 power the beak during forceful biting. Increased integration between the beak and braincase
170 may therefore facilitate improved feeding performance in both the beak and the rest of the
171 skull in Hawaiian honeycreepers and in Darwin's finches, for whom a demonstrated link
172 between beak morphology and feeding exists⁴⁰. This directional evolution may also have
173 produced some of the highest values of total craniofacial disparity at the family/subfamily
174 level for both clades (Fig. 4b), which is particularly striking considering that Darwin's
175 finches and Hawaiian honeycreepers are substantially younger than most of the other
176 considered families (Fig.4c). Therefore, the constrained (Figs. 3, 4b & 4d, Table 1, Extended
177 Data. Fig. 7), but morphologically extreme (Figs. 2 & 4c) and rapid (Fig. 2), craniofacial
178 evolution in Darwin finches and Hawaiian honeycreepers meets the expectations of rapid
179 evolution along lines of phenotypic least resistance^{17,23}, where high integration, rather than
180 high modularity, facilitates evolution along a particular adaptive morphocline.

181 Rapid evolution along lines of phenotypic least resistance may also explain the
182 apparent contradiction between large phenotypic divergence despite little change in genetic
183 divergence between species in Darwin's finches and in Hawaiian honeycreepers^{3,5}. It may
184 also shed some light on why other passerine lineages that colonized both archipelagos at
185 similar times failed to undergo the same explosive adaptive radiation. In Hawaii, the two
186 endemic lineages of passerine birds that colonized the archipelago at similar times to
187 Hawaiian honeycreepers are the Hawaiian thrushes (5 species, Turdidae)⁵, and the extinct
188 Hawaiian honeyeaters (5 species, Mohoidae)¹⁰. Both families belong to the parvorder
189 Muscicapida, the passerine lineage exhibiting the lowest integration in our data (Fig. 4a).
190 Similarly, the other endemic radiation in the Galapagos archipelago, the Galapagos
191 mockingbirds (4 species, Mimidae, also in the Muscicapida), colonised the islands at a
192 similar time but did not undergo a rapid diversification⁴. While multiple ecologically relevant
193 traits of the colonizer species may have contributed to the diversification patterns of
194 passerines in Galapagos and Hawaii, we suggest that their lower craniofacial integration may
195 have been an important factor preventing them exploiting adaptive lines of least resistance
196 that likely produced the rapid and large evolutionary change in cranial morphology that we
197 showed in Darwin's finches and Hawaiian honeycreepers. Nonetheless, our study
198 demonstrates that adaptive radiations are possible under tighter cranial integration.

199 In summary, we propose that a stronger craniofacial integration was a key factor
200 shaping the extreme craniofacial evolution of two classic radiations of island passeroids.
201 While an intrinsic evolutionary lability of the beak has been proposed for several families of
202 passeroid songbirds^{5,31,32,40}, other studies have shown that beak shape among the group is
203 constrained to a small series of shape transformations arising from a constrained
204 morphogenetic program⁴¹. Our hypothesis reconciles both views by showing that although
205 high cranial integration constrains the shapes of the beak and skull, it may also facilitate
206 evolutionary lability along specific phenotypic clines in particular ecological scenarios.

207 **Acknowledgements**

208 We are thankful to Joanne Cooper and Judith White
209 (NHM Tring), and Christopher M. Milensky and Brian K. Schmidt (Smithsonian National
210 Museum of Natural History) for access to specimens. We thank Fernando Blanco, Matteo
211 Fabbri, Iris Menéndez, and Luis Porras for enlightening discussion on the evolutionary
212 implications of this research. We are grateful to Gavin Thomas, Thomas Püschel, Chris
213 Klingenberg, Armin Elsler, Frane Babarović and Soledad de Esteban-Trivigno for
214 enlightening insights and discussion on the methods. We thank Óscar Sanisidro and Lucía
215 Balsa Pascual for design and technical advice that greatly improved the quality of the graphic
216 support. GN was supported by a PG Scholarship/Studentship from The Alumni Foundation,
217 University of Bristol, UK and is currently supported by the ERC project ‘TEMPO’ (grant
218 number: 639791). JML is supported by the Spanish MINECO, Project CGL-2013-42643.
219 EJ R and JAB were supported by a BBSRC grant BB/I011668/1.

220 **Author’s contributions**

221 The focus and design of this research was developed by GN, JM-L, JAB and ERJ. CRC
222 conducted the Variable Rates Model Analyses. GN conducted the remaining of the analyses.
223 GN JM-L, JAB, CRC and ERJ co-wrote the manuscript.

224 **Competing interests**

225 The authors declare no competing financial interests.

226

227 **METHODS**

228 **Database and phylogenetic hypothesis**

229 Our study includes 128 families of landbirds (i.e: Inopinaves, defined as Telluraves
230 (Yuri et al. 2013) + *Opisthocomus hoazin*, Prum et al. 2015) giving a total of 436 species
231 (Supplementary Data 5. List of specimens). All but five families within the landbird radiation
232 are represented in our sample (Philepittidae, Sapayoidae, Dasyornithidae, Urocynchramidae
233 and Aegithinidae). These families are either monotypic or have an extremely reduced
234 diversity, and often regarded as belonging within other passerine families⁴⁴. Sampling was
235 non-random and aimed to capture the maximum beak morphological disparity within each
236 family, with a special focus on the subfamilies of Darwin’s finches (Geospizinae) and
237 Hawaiian honeycreepers (Drepanidinae) (represented in our sample by ~70% and ~ 60 % of
238 their extant diversity, respectively). A time-calibrated maximum clade credibility (MCC)
239 phylogeny of the 436 species was generated using TreeAnnotator⁴⁵ from a population of
240 10,000 ‘Hackett’s backbone stage 2 trees’. Trees were generated using the in-built tools from
241 www.birdtree.org (for full details regarding tree construction methods, see¹), and branch
242 lengths were set equal to ‘Common ancestor’ node heights. The resulting MCC phylogeny is
243 largely congruent with the last genomic phylogenies for the interrelationships of landbirds
244 (Figs. 2, 4a & 4b,^{28,29}).

245 **Geometric morphometrics**

246 A set of 17 landmarks and 2 curves (three evenly separated semilandmarks along the
247 dorsal and ventral rims of the beak) was digitized using the software tpsDig.2⁴⁶ in lateral
248 views of the skull of each specimen (Extended Data Fig. 1, Landmark position/ Extended
249 Data. Fig. 2, Landmark definition). The Minimum Bending Energy criterion was applied to
250 slide the semilandmarks in tpsRelw⁴⁷, as this is more appropriate than the Minimum
251 Procrustes Distance criterion when dealing with data with high morphological variation in the
252 software used here⁴⁸. Landmarks and semilandmarks were then classified as belonging to the
253 ‘beak block’ (block 1) or ‘skull block’ (block 2) (Extended Data Figs. 1 & 2). Shape data
254 (Procrustes coordinates) was extracted using three different full Generalized Procrustes
255 Analyses (GPAs) for: 1) the whole landmark configuration; 2) the ‘beak block’; and 3) the
256 ‘skull block’. An additional Generalized Resistant Procrustes Superimposition (GRPS,⁴⁹) was
257 conducted in the raw coordinates from the whole landmark configuration to identify possible
258 trait-correlation artefacts in our shape data (see Methods. Evolutionary covariation & SI).
259 GPA aligned Procrustes coordinates were thereafter imported to MorphoJ⁵⁰ and the R
260 statistical environment⁵¹ for all downstream analyses.

261 **Principal Component Analyses (PCA) and Variable Rates Model Analyses (VRMA)**

262 To explore the main patterns of skull shape variation in landbirds, we conducted
263 Principal Component Analyses (PCAs) for: 1) the whole configuration; 2) the ‘beak block’;
264 and 3) the ‘skull block’. The time-calibrated MCC phylogeny was mapped over the PCAs by
265 weighted (i.e., including branch length information) square-change parsimony in order to
266 visualize evolutionary changes over the morphospace. Principal Components Analyses
267 (including mapping time calibrated trees) were conducted in MorphoJ.

268 To explore the tempo of craniofacial evolution in landbirds, we used the scores
269 derived from the previous PCAs to conduct Variable Rates Model Analyses (VRMAs) using
270 the software BayesTraits V2.0.2⁵² (available from <http://www.evolution.rdg.ac.uk/>). This
271 method uses a reversible jump Markov chain Monte Carlo (MCMC) approach to estimate the
272 location, probability, and magnitude of rate shifts in continuous traits across branches of a
273 phylogenetic tree (see⁵³). We used PC scores for: 1) the whole skull (13 PCs); 2) the ‘beak
274 block’ (6 PCs); and 3) the ‘skull block’ (10 PCs). We used the number of principal
275 components that account for 95% of shape variance, except for the whole configuration
276 where we used the number that account for 90% to avoid poor performance due to a high
277 number of variables⁵⁴. We ran two replicate chains for each model using default priors and
278 assuming uncorrelated trait axes². Each chain was run for 200,000,000 iterations (sampled
279 every 10,000 iterations), with the first 100,000,000 iterations removed as burn in. We
280 confirmed that replicate runs had converged and combined the output of both runs for further
281 analysis. We summarized the results of each run by calculating (1) the mean rate, and (2) the
282 probability of a rate shift (branch or clade) over all posterior samples for each node in the
283 tree. In the main text, we focus on rate shifts that are inferred with higher posterior
284 probability (PP) than 0.70. To account for rate heterogeneity in downstream analyses of
285 evolutionary covariation (see Methods. Evolutionary covariation and SI), a rate-scaled
286 phylogeny (non-ultrametric) was generated by using the branch lengths predicted by the
287 model of the VRMA conducted with the whole skull configurations.

288 **Evolutionary covariation**

289 Evolutionary covariation between the ‘beak block’ (block 1) and the ‘skull block’
290 (block 2) was examined for each of the clades of landbirds by means of Phylogenetic Partial
291 Least Squares analysis (P-PLS,^{55,56}) in three different situations: two blocks using the
292 calibrated time tree (separate GPA for the ‘beak block’ and the ‘skull block’) (situation 1);
293 two blocks using the rate-scaled phylogeny (situation 2); and within one configuration (one
294 single GPA for the whole configuration) using the rate-scaled tree (situation 3). Phylogenetic
295 Partial Least Squares (P-PLS) is a multivariate analysis that quantifies the evolutionary
296 covariation between two different sets of data by searching for vectors of correlated variables
297 without implying predictability of one set of variables upon the other.

298 Although least-squares GPA⁵⁷ provides a universal criterion for defining shape data,
299 and convenient statistical properties for downstream multivariate analyses that other
300 superimposition methods do not⁵⁸, it has some widely recognised limitations when shape
301 differences between landmarks are highly heterogeneous^{49,59-61}. This is because GPA
302 assumes that variation among landmarks is homogeneous and that all landmarks vary
303 isotropically⁵⁷ (they are equally distributed in all directions). Therefore, if a great deal of the
304 total shape difference is concentrated in just a few landmarks, and/or its variation is skewed
305 towards one or more directions, GPA tends to spread this localized shape variance across the
306 whole configuration, generating artefactual shape differences^{49,61-63} (i.e., the ‘Pinocchio
307 effect’⁶²). This issue can be particularly misleading when evaluating covariation patterns (i.e.
308 integration and modularity) as it tends to overestimate integration. There is still debate as to
309 whether this is a critical concern in real biological data or not^{49,61,64}, however, in an
310 exploratory study Cardini⁶¹, showed that GPA can generate artefactual patterns of covariation
311 even if the original shape data exhibits no covariation at all. The fact that landbirds
312 demonstrate high beak shape variation relative to other skull regions^{25,34} led us to
313 contemplate this possibility. Therefore, to identify whether the aforementioned might be a
314 problem in our sample, we carried out a Generalized Resistant Procrustes Superimposition
315 (GRPS^{49,60}) in the raw coordinates (unaligned) for the whole configurations for all landbirds
316 and compared them with a GPA superimposition using Resistant Procrustes Software (RPS⁴⁹,
317 available online at: <https://sites.google.com/site/resistantprocrustes/>) (SI. 4). GPRS differs
318 from GPA in that the set of criteria for eliminating rotational information from shape data are
319 estimated through a repeated-medians calculation for each dataset, rather than minimizing the
320 squared sum of Euclidean distances between the landmark coordinates⁶⁰. This criterion is
321 therefore robust to larger variation in a few landmarks with respect to the whole
322 configuration, and thus better portrays localized variation across coordinates^{49,60}.
323 Additionally, we tested evolutionary shape covariation between blocks 1 and 2 within one
324 configuration (situation 3, single GPA) to gain insight on how localized variation might affect
325 integration results in our sample (SI. Expanded Results, SI. Figs. 5 & 6; SI. Table 2).

326 Because GPRS and other resistant-based procedures are not based in Procrustes
327 distances, concerns have been expressed regarding their ability to generate shape tangent
328 spaces appropriate for Euclidean multivariate statistics (e.g.,⁶⁵). Although there are
329 specifically implemented multivariate methods for dealing with data extracted from a GPRS,

330 the standard usage of GPA in modern geometric morphometrics^{66,67} means that most
331 available methods are based on Procrustes distances. These Procrustes-based analyses need
332 the consistency with the Procrustes projection that defines shape variables in geometric
333 morphometrics⁵⁸. To our knowledge, there is not currently an appropriate method able to
334 overcome both trait correlation artefacts yet retain an equivalence with Euclidean
335 multivariate statistics. Consequently, we are forced to quantify covariation using two blocks
336 (situations 1 and 2) in an attempt to mitigate any artefactual spread of variance across the
337 whole configuration (see SI. Expanded Results for further details). This approach is better at
338 portraying the original patterns of local variation in geometric morphometrics and generally
339 eliminate artefactual trait covariation, at least as far as integration is concerned⁶¹. However,
340 covariation in situations 1 and 2 only reflects evolutionary shape covariation, as information
341 regarding relative size and arrangement between blocks is lost (eliminated in each block's
342 separate GPA) and can only be accessed indirectly (e.g., because the shape data is a 2-
343 dimensional projection of a 3D object, certain shape changes might be indicative of
344 differences in arrangement angle).

345 Several studies have shown that landbirds exhibit extreme heterogeneity of rates of
346 craniofacial evolution^{2,25}, which we also quantified here (Fig 2; SI. Tables 1-3). Computation
347 of Phylogenetic Partial Least Squares in *geomorph*⁶⁸ assumes a single-rate Brownian Motion
348 model of evolution which is unlikely to conform to shape data that evolved with highly
349 heterogeneous rates. When shape data does not conform to a single-rate BM model, previous
350 approaches rescaled the branch lengths of the phylogeny using the parameters estimated by
351 the model that best fits the data from a selection of *a priori* models, namely: single-rate BM,
352 Ornstein-Uhlenbeck, and Early-Burst (e.g.⁶⁹). This approach coerces the phylogenetic
353 covariation matrix to approximate a BM model, therefore meeting the expectations of the
354 analysis. However, recent research has shown that current model-fitting methods based on
355 maximum-likelihood tend to exhibit ill-conditioned covariation matrices, leading to
356 misidentifications of the model of evolution⁵⁴, even when the data is generated under a
357 particular model like BM⁷⁰. Here, we chose a different approach: we used the branch lengths
358 estimated by the VRMA for the whole skull configuration. In this way, we rescaled the
359 branch lengths in our tree to account for the actual rates of phenotypic evolution rather than
360 using parameters estimated by the fit to a particular set of *a priori* single-process models.
361 Although this solution is not ideal, it allows for the inclusion of branch lengths estimated by
362 more complex models than previous approaches, which have also been shown to exhibit best
363 fits for other cases of trait evolution like body mass⁷¹. The methodological endeavour needed
364 to implement more complex evolutionary models in phylogenetic comparative methods for
365 high dimensional data⁷² goes well beyond the scope of this study. Here, comparisons between
366 situations 1 (two blocks using the calibrated time tree) and 2 (two blocks using the rate-scaled
367 tree) aimed to gain insight on the effects of accounting for variable rates in evolutionary
368 covariation in measures of evolutionary integration (SI. Figs. 2 & 3; Supplementary Data 3).

369 The strength of evolutionary covariation in each of the three scenarios was compared
370 and tested between major radiations of landbirds and between the major radiations of
371 passerines following a recently developed statistical procedure⁷³. The major non-passerine

372 radiations were compared to the major subdivisions of the Passeriformes (Passeri and
373 Tyranni) based on the high support in all the latest phylogenetic hypotheses of these clades
374 and similar node age estimations²⁹. The more recently-branching passerine parvorders were
375 compared between each other. As P-PLS correlation values (*rpls*) have been shown to be
376 influenced by sample size⁷⁴, comparing or testing for differences in integration levels
377 between two different sample sizes using this statistic is problematic. Adams & Collyer⁷³
378 recently proposed the use of *rpls* effects sizes (z-scores). Z-scores were therefore calculated
379 as the standard deviates of the *rpls* values from the permutation procedure for the P-PLS
380 analyses of each clade, and confidence intervals were calculated for each value. Pairwise
381 differences in z-scores were then compared and statistically tested in order to discriminate
382 between levels of integration between clades. Z-score values were used directly to elucidate
383 which clades exhibited higher integration when differences were found. To explore the
384 differences in the pattern of cranial integration between clades, pairwise angles and
385 correlations of PLS1 vectors (the pair of vectors that covary most for each P-PLS) were
386 calculated for all the clades in situation 2 (Extended Data Fig. 6; Extended Data Fig. 10; SI.
387 Fig. 1; Supplementary Data 1 & 2). Histograms of frequency of binned angles and shape
388 differences across each vector were plotted for visual comparisons (Extended Data Fig. 6; SI.
389 Fig. 1).

390 Finally, we addressed whether stronger cranial integration generated greater
391 morphological change along the evolutionary line of least resistance in Darwin's finches and
392 Hawaiian honeycreepers than in other landbird families. To do so, we computed maximum
393 distances within each family (or subfamily for Geospizinae and Drepanidinae) of landbirds
394 for the PLS1 scores of the beak and skull blocks as a proxy of the degree of spread along the
395 line of least resistance. We did this for the PLS1 axes defined for each order (and Passeri and
396 Tyranni for the Passeriformes) and compared PLS1 distances for the beak and skull block
397 between all the families. Furthermore, we repeated this for the parvorder Passerida and
398 compared PLS1 distances for the beak and skull block between passeroid families alone. To
399 ascertain whether a larger spread across the lines of least resistance also corresponds to more
400 extreme cranial morphologies, we computed maximum Procrustes distances within each
401 family/subfamily using the Procrustes coordinates (both from the whole configuration and
402 beak and skull blocks separately).

403 **Data availability**

404 All relevant data is available via the University of Bristol's DataBris repository at
405 <https://data.bris.ac.uk/data/dataset/3kpwgpnqewcy2tvak6uzzdztt>.

406 **Literature**

- 407 1 Jetz, W., Thomas, G., Joy, J., Hartmann, K. & Mooers, A. The global diversity of birds in space
408 and time. *Nature* **491**, 444-448 (2012).
- 409 2 Cooney, C. R. *et al.* Mega-evolutionary dynamics of the adaptive radiation of birds. *Nature*
410 **542**, 344-347 (2017).
- 411 3 Burns, K. J., Hackett, S. J. & Klein, N. K. Phylogenetic relationships and morphological
412 diversity in Darwin's finches and their relatives. *Evolution* **56**, 1240-1252 (2002).

413 4 Arbogast, B. S. *et al.* The origin and diversification of Galapagos mockingbirds. *Evolution* **60**,
414 370-382 (2006).

415 5 Lovette, I. J., Bermingham, E. & Ricklefs, R. E. Clade-specific morphological diversification
416 and adaptive radiation in Hawaiian songbirds. *Proceedings of the Royal Society of London B:*
417 *Biological Sciences* **269**, 37-42 (2002).

418 6 Pratt, H. D. & Conant, S. *The Hawaiian Honeycreepers: Drepanidinae.* (Oxford University
419 Press, 2005).

420 7 Tokita, M., Yano, W., James, H. F. & Abzhanov, A. Cranial shape evolution in adaptive
421 radiations of birds: comparative morphometrics of Darwin's finches and Hawaiian
422 honeycreepers. *Phil. Trans. R. Soc. B* **372**, 20150481 (2017).

423 8 Darwin, C. *The Zoology of the Voyage of HMS Beagle: Under the Command of Captain*
424 *Fitzroy, RN, During the Years 1832 to 1836: Published with the Approval of the Lords*
425 *Commissioners of Her Majesty's Treasury.* (Smith, Elder and Company, 1839).

426 9 Mayr, E. The zoogeographic position of the Hawaiian Islands. *The Condor* **45**, 45-48 (1943).

427 10 Fleischer, R. C., James, H. F. & Olson, S. L. Convergent evolution of Hawaiian and Australo-
428 Pacific honeyeaters from distant songbird ancestors. *Current Biology* **18**, 1927-1931 (2008).

429 11 Bright, J. A., Marugán-Lobón, J., Cobb, S. N. & Rayfield, E. J. The shapes of bird beaks are
430 highly controlled by nondietary factors. *Proceedings of the National Academy of Sciences*,
431 201602683 (2016).

432 12 Abzhanov, A. The old and new faces of morphology: the legacy of D'Arcy Thompson's 'theory
433 of transformations' and 'laws of growth'. *Development* **144**, 4284-4297 (2017).

434 13 Goswami, A., Smaers, J., Soligo, C. & Polly, P. The macroevolutionary consequences of
435 phenotypic integration: from development to deep time. *Philosophical Transactions of the*
436 *Royal Society of London B: Biological Sciences* **369**, 20130254 (2014).

437 14 Klingenberg, C. P. Studying morphological integration and modularity at multiple levels:
438 concepts and analysis. *Philosophical Transactions of the Royal Society of London B: Biological*
439 *Sciences* **369**, 20130249 (2014).

440 15 Felice, R. N., Randau, M. & Goswami, A. A fly in a tube: Macroevolutionary expectations for
441 integrated phenotypes. *Evolution* **72**, 2580-2594 (2018).

442 16 Olson, E. C. & Miller, R. L. *Morphological integration.* (University of Chicago Press, 1999).

443 17 Villmoare, B. Morphological integration, evolutionary constraints, and extinction: a
444 computer simulation-based study. *Evolutionary Biology* **40**, 76-83 (2013).

445 18 Fisher, R. A. *The genetic theory of natural selection.* (Dover, 1958).

446 19 Kirschner, M. & Gerhart, J. Evolvability. *Proceedings of the National Academy of Sciences* **95**,
447 8420-8427 (1998).

448 20 Wagner, G. P. & Altenberg, L. Perspective: complex adaptations and the evolution of
449 evolvability. *Evolution* **50**, 967-976 (1996).

450 21 Raff, R. A. *The shape of life: genes, development, and the evolution of animal form.*
451 (University of Chicago Press, 2012).

452 22 Wagner, G. Coevolution of functionally constrained characters: prerequisites for adaptive
453 versatility. *BioSystems* **17**, 51-55 (1984).

454 23 Marroig, G. & Cheverud, J. M. Size as a line of least evolutionary resistance: diet and
455 adaptive morphological radiation in New World monkeys. *Evolution* **59**, 1128-1142 (2005).

456 24 Hansen, T. F. Is modularity necessary for evolvability?: Remarks on the relationship between
457 pleiotropy and evolvability. *Biosystems* **69**, 83-94 (2003).

458 25 Felice, R. N. & Goswami, A. Developmental origins of mosaic evolution in the avian cranium.
459 *Proceedings of the National Academy of Sciences*, 201716437 (2018).

460 26 Bright, J. A., Marugán-Lobón, J., Rayfield, E. J. & Cobb, S. N. The multifactorial nature of beak
461 and skull shape evolution in parrots and cockatoos (Psittaciformes). *BMC evolutionary*
462 *biology* **19**, 104 (2019).

463 27 Hackett, S. J. *et al.* A phylogenomic study of birds reveals their evolutionary history. *science*
464 **320**, 1763-1768 (2008).

465 28 Jarvis, E. D. *et al.* Whole-genome analyses resolve early branches in the tree of life of
466 modern birds. *Science* **346**, 1320-1331 (2014).

467 29 Prum, R. O. *et al.* A comprehensive phylogeny of birds (Aves) using targeted next-generation
468 DNA sequencing. *Nature* (2015).

469 30 Gibbs, H. L. & Grant, P. R. Oscillating selection on Darwin's finches. (1987).

470 31 Grant, P. R. & Grant, B. R. Evolution of character displacement in Darwin's finches. *science*
471 **313**, 224-226 (2006).

472 32 Smith, T. B., Freed, L. A., Lepson, J. K. & Carothers, J. H. Evolutionary consequences of
473 extinctions in populations of a Hawaiian honeycreeper. *Conservation Biology* **9**, 107-113
474 (1995).

475 33 Darwin, C. & Wallace, A. On the tendency of species to form varieties; and on the
476 perpetuation of varieties and species by natural means of selection. *Zoological Journal of the*
477 *Linnean Society* **3**, 45-62 (1858).

478 34 Klingenberg, C. P. Cranial integration and modularity: insights into evolution and
479 development from morphometric data. *Hystrix, the Italian Journal of Mammalogy* **24**, 43-58
480 (2013).

481 35 Schluter, D. Adaptive radiation along genetic lines of least resistance. *Evolution* **50**, 1766-
482 1774 (1996).

483 36 Randau, M. & Goswami, A. Unravelling intravertebral integration, modularity and disparity in
484 Felidae (Mammalia). *Evolution & development* **19**, 85-95 (2017).

485 37 Losos, J. B. & Ricklefs, R. E. Adaptation and diversification on islands. *Nature* **457**, 830 (2009).

486 38 Wright, N. A., Steadman, D. W. & Witt, C. C. Predictable evolution toward flightlessness in
487 volant island birds. *Proceedings of the National Academy of Sciences*, 201522931 (2016).

488 39 van der Geer, A. A., Lyras, G. A., Mitteroecker, P. & MacPhee, R. D. From Jumbo to Dumbo:
489 Cranial Shape Changes in Elephants and Hippos During Phyletic Dwarfing. *Evolutionary*
490 *Biology*, 1-15 (2018).

491 40 Grant, B. R. & Grant, P. R. Evolution of Darwin's finches caused by a rare climatic event.
492 *Proceedings of the Royal Society of London B: Biological Sciences* **251**, 111-117 (1993).

493 41 Fritz, J. A. *et al.* Shared developmental programme strongly constrains beak shape diversity
494 in songbirds. *Nature communications* **5** (2014).

495 42 Marroig, G., Shirai, L. T., Porto, A., de Oliveira, F. B. & De Conto, V. The evolution of
496 modularity in the mammalian skull II: evolutionary consequences. *Evolutionary Biology* **36**,
497 136-148 (2009).

498 43 Renaud, S., Auffray, J. C. & Michaux, J. Conserved phenotypic variation patterns, evolution
499 along lines of least resistance, and departure due to selection in fossil rodents. *Evolution* **60**,
500 1701-1717 (2006).

501 44 Del Hoyo, J. *et al.* Handbook of the Birds of the World Alive. Lynx Editions, Barcelona.
502 (2017).

503 45 Rambaut, A. & Drummond, A. TreeAnnotator v1. 7.0. Available as part of the BEAST package
504 at <http://beast.bio.ed.ac.uk> (2013).

505 46 Rohlf, F. tpsDig, version 2.10. Department of Ecology and Evolution, State University of New
506 York, Stony Brook (2006).

507 47 Rohlf, F. tpsRelw, relative warps analysis. Department of Ecology and Evolution, State
508 University of New York at Stony Brook, Stony Brook, NY (2010).

509 48 Perez, S. I., Bernal, V. & Gonzalez, P. N. Differences between sliding semi-landmark methods
510 in geometric morphometrics, with an application to human craniofacial and dental variation.
511 *Journal of anatomy* **208**, 769-784 (2006).

512 49 Torcida, S., Perez, S. I. & Gonzalez, P. N. An integrated approach for landmark-based
513 resistant shape analysis in 3D. *Evolutionary Biology* **41**, 351-366 (2014).

514 50 Klingenberg, C. MorphoJ. *Faculty of Life Sciences, University of Manchester* **3**, 75-77 (2008).
515 51 Team, R. C. (2017).
516 52 Pagel, M. & Meade, A. BayesTraits v. 2.0. *Reading: University of Reading* (2013).
517 53 Venditti, C., Meade, A. & Pagel, M. Multiple routes to mammalian diversity. *Nature* **479**, 393
518 (2011).
519 54 Adams, D. C. & Collyer, M. L. Multivariate phylogenetic comparative methods: evaluations,
520 comparisons, and recommendations. *Systematic biology* **67**, 14-31 (2017).
521 55 Adams, D. C. & Felice, R. N. Assessing trait covariation and morphological integration on
522 phylogenies using evolutionary covariance matrices. *PloS one* **9**, e94335 (2014).
523 56 Rohlf, F. J. & Corti, M. Use of two-block partial least-squares to study covariation in shape.
524 *Systematic Biology*, 740-753 (2000).
525 57 Rohlf, F. J. & Slice, D. Extensions of the Procrustes method for the optimal superimposition
526 of landmarks. *Systematic Biology* **39**, 40-59 (1990).
527 58 Bookstein, F. L. in *Advances in morphometrics* 131-151 (Springer, 1996).
528 59 Dryden, I. & Mardia, K. *Statistical analysis of shape*. (Wiley, 1998).
529 60 Siegel, A. F. & Benson, R. H. A robust comparison of biological shapes. *Biometrics*, 341-350
530 (1982).
531 61 Cardini, A. Integration and modularity in Procrustes shape data: is there a risk of spurious
532 results? *Evolutionary Biology*, 1-16 (2018).
533 62 Chapman, R. E. in *Proceedings of the Michigan morphometrics workshop*. (University of
534 Michigan Museum of Zoology, Ann Arbor).
535 63 Zelditch, M. L., Swiderski, D. L. & Sheets, H. D. *Geometric morphometrics for biologists: a*
536 *primer*. (Academic Press, 2012).
537 64 Klingenberg, C. P. & McIntyre, G. S. Geometric morphometrics of developmental instability:
538 analyzing patterns of fluctuating asymmetry with Procrustes methods. *Evolution* **52**, 1363-
539 1375 (1998).
540 65 Bookstein, F. L. in *Image Fusion and Shape Variability Techniques*. 59-70 (Leeds: Leeds
541 University Press).
542 66 Adams, D. C., Rohlf, F. J. & Slice, D. E. A field comes of age: geometric morphometrics in the
543 21st century. *Hystrix* **24**, 7 (2013).
544 67 Adams, D. C., Rohlf, F. J. & Slice, D. E. Geometric morphometrics: ten years of progress
545 following the 'revolution'. *Italian Journal of Zoology* **71**, 5-16 (2004).
546 68 Adams, D. C., Collyer, M. L. & Kaliontzopoulou, A. (2018).
547 69 Zelditch, M. L., Ye, J., Mitchell, J. S. & Swiderski, D. L. Rare ecomorphological convergence on
548 a complex adaptive landscape: body size and diet mediate evolution of jaw shape in squirrels
549 (Sciuridae). *Evolution* **71**, 633-649 (2017).
550 70 Uyeda, J. C., Caetano, D. S. & Pennell, M. W. Comparative analysis of principal components
551 can be misleading. *Systematic Biology* **64**, 677-689 (2015).
552 71 Chira, A. M. & Thomas, G. H. The impact of rate heterogeneity on inference of phylogenetic
553 models of trait evolution. *Journal of evolutionary biology* **29**, 2502-2518 (2016).
554 72 Monteiro, L. R. Morphometrics and the comparative method: studying the evolution of
555 biological shape. *Hystrix, the Italian Journal of Mammalogy* **24**, 25-32 (2013).
556 73 Adams, D. C. & Collyer, M. L. On the comparison of the strength of morphological integration
557 across morphometric datasets. *Evolution* **70**, 2623-2631 (2016).
558 74 Mitteroecker, P. & Bookstein, F. The conceptual and statistical relationship between
559 modularity and morphological integration. *Systematic biology* **56**, 818-836 (2007).

560

561

562

563

564

565

566

567 **Figures legends:**

568 **Figure 1. How integration and selection direct phenotypic evolution.** a) Approximate areas of simulated
569 phenotypic evolution for high (dark grey ellipse) and zero (light grey circle) trait-covariation (modified from ¹³).
570 Higher integration entails exploration of more extreme trait values (following ¹⁷); b) A complete modular
571 organization between beak and skull shape (i.e. zero covariation) representing the extreme scenario of the
572 condition proposed for the classic passerine adaptive radiations whereby the beak can evolve more freely ^{7,11,12}.
573 This scenario permits the initial theoretical phenotype (small dark grey ellipse) reaching all three theoretical
574 adaptive peaks (white ellipses), allowing greater evolutionary flexibility (e.g. ^{13,42}); c) The alternative scenario,
575 an integrated organization between beak and skull shape (i.e. stronger covariation) strongly facilitates reaching
576 the theoretical adaptive peak that is aligned with the axis of maximum phenotypic covariation (i.e. phenotypic
577 line of least resistance, *sensu* ²³) to the detriment of the adaptive peaks that are not aligned with this axis ^{17,23,24}.
578 Boundary lines are dashed to reflect that phenotypic evolution is more likely to happen within the area described
579 by the covariation structure (yellow area) but can occur beyond those limits (greenish blue background), for
580 instance if directional selection is strong enough (e.g. ⁴³).

581 **Figure 2. Pattern and tempo of craniofacial evolution in landbirds.** Phylomorphospaces of the first three
582 principal components of shape (left), shape changes associated with these shape axes (centre), and rates of
583 morphological evolution (right) for a) the whole skull; (b) 'beak'; and (c) 'skull' blocks. Light grey convex hull
584 encloses Passeriformes, dark grey convex hull encloses Psittaciformes; purple dots represent Darwin's finches
585 and pink dots represent Hawaiian honeycreepers (see Extended Data Figs 3-5 for the main landbird orders
586 labelled in the phylomorphospaces). Branch colours in the phylogenies indicate relative rate of evolution.
587 Inferred rate shifts with higher posterior probability than 0.7 are plotted in corresponding branches (circles) or
588 nodes (triangles) in the phylogeny (see SI. Tables 1-3 for the full list of rate shifts). Posterior probability of each
589 inferred rate shift is indicated by the size of said circle or triangle. Clade labels as in Figs. 3,4 and Table 1.

590 **Figure 3. Evolutionary integration between the beak and the skull in landbirds.** PLS1 plots for the Two
591 Blocks-Phylogenetic Partial Least Squares Analyses using the rate-scaled phylogeny (situation 2, see Methods)
592 in each clade (numbers correspond to clades as detailed in Table 1). Y axes show PLS1 scores beak block; X
593 axes show PLS1 scores skull block. a) Major landbird lineages, b) major lineages of passerines. Purple dots
594 represent Darwin's finches and pink dots represent Hawaiian honeycreepers.

595 **Figure 4. Strength of cranial integration across landbirds and maximum phenotypic distances per**
596 **family/subfamily.** a) Z-scores and corresponding intervals of confidence for each major lineage of landbirds
597 and (b) passerine parvorder. Z-scores are effect sizes from the randomized distribution of *rpls* values from the
598 phylogenetic PLS for each clade (situation 2, two blocks, using the rate-scaled phylogeny; see Methods).
599 Cladograms portray the simplified phylogenetic relationships of the main landbird lineages in our phylogeny
600 (solid colours) as compared to other recently published phylogenetic hypothesis²⁹(transparent colour). (b)
601 Brighter silhouettes represent the island passeroids Darwin's finches (purple) and Hawaiian honeycreepers
602 (pink), whereas less contrasted silhouettes represent the island muscicapoids that radiated in Galapagos (greyish
603 purple) and Hawaii (greyish pink). Our phylogeny is exactly coincident with Prum et al.'s²⁹ for the
604 interrelationship of major passerine lineages. c) Maximum total Procrustes distances per family/subfamily for
605 the 'beak' and the 'skull' blocks. d) Maximum PLS1 distances per family/subfamily for the 'beak' and 'skull'
606 block. Labels in c and d correspond to families as detailed in Extended Data Fig. 9. Dot colours in c and d

607 correspond to the ages of the most common recent ancestor (MRCA) for each of the focal families in our MCC

Main landbird lineages

608 tree.

609

610

611

612

613 **Tables**

614

615 **Table 1.** Pairwise comparisons of z-scores (strength of evolutionary covariation between beak and skull)
616 between clades and associated *P* values for situation 2 (two blocks, using the rate-scaled phylogeny, see
617 Methods). Bold values are statistically significant ($P < 0.05$). Each clade z-score value is provided. 1*Passerida
618 = Passerida excluding Darwin's finches and Hawaiian honeycreepers.

619

620

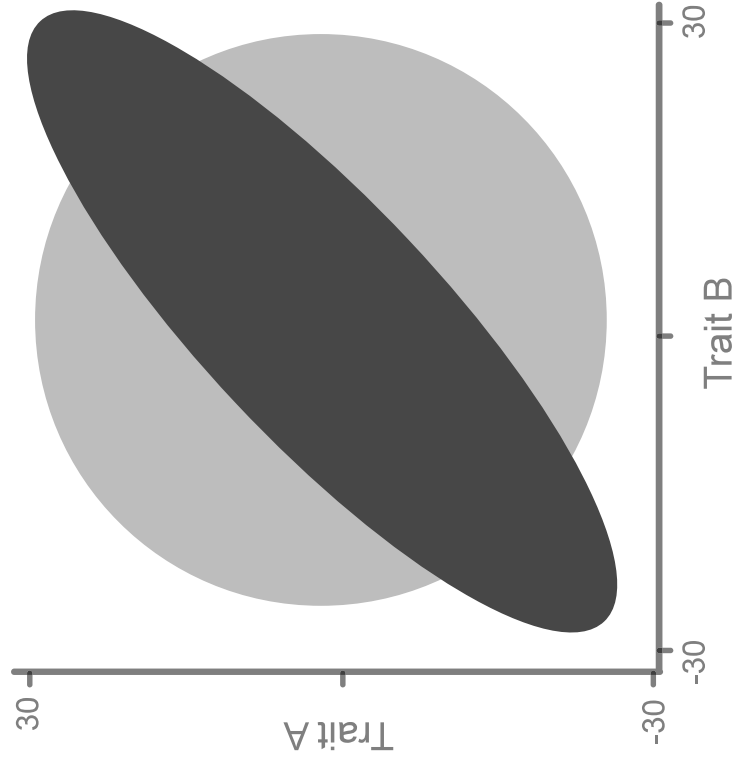
621

622

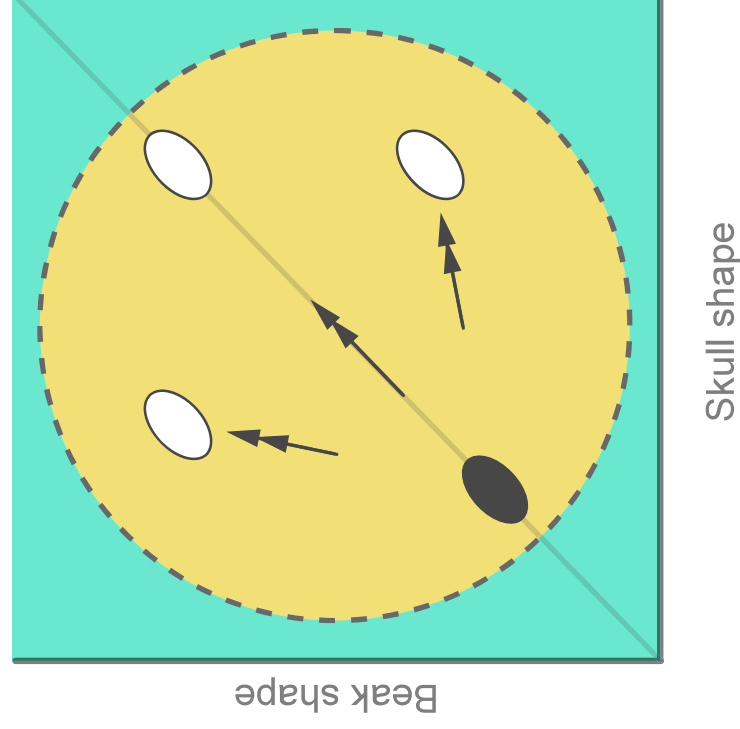
Z (means)	Clades	1	2	3	4	5	6	7	8	9	10	11	12	13
10.25	1. All landbirds													
5.47	2. Non-Passerines	0.0196												
7.62	3. Passeriformes	0.4057	0.0245											
5.63	4. Passeri	0.2287	0.1715	0.1986										
2.71	5. Tyranni	0.0943	0.4649	0.0847	0.2324									
5.03	6. Psittaciformes	0.2087	0.0250	0.2683	0.1147	0.0532								
0.24	7. Falconiformes	0.0016	0.0301	0.0017	0.0091	0.0642	0.0015							
0.80	8. Piciformes	0.0003	0.0237	0.0005	0.0052	0.0720	0.0008	0.3873						
0.76	9. Coraciiformes	0.0033	0.0584	0.0034	0.0182	0.1103	0.0031	0.3675	0.4652					
1.38	10. Bucerotiformes	0.0183	0.1643	0.0172	0.0642	0.2292	0.0125	0.2224	0.2814	0.3272				
1.36	11. Trogoniformes	0.0083	0.1189	0.0083	0.0402	0.1885	0.0069	0.2420	0.3087	0.3564	0.4609			
1.21	12. Eucavitaves	0.0001	0.0165	0.0001	0.0029	0.0719	0.0004	0.3380	0.4453	0.4898	0.3074	0.3389		
1.26	13. Strigiformes	0.0071	0.1066	0.0071	0.0354	0.1740	0.0061	0.2598	0.3318	0.3781	0.4391	0.4769	0.3648	
0.83	14. Accipitriformes	0.0008	0.0345	0.0010	0.0086	0.0865	0.0013	0.3716	0.4775	0.4862	0.3038	0.3326	0.4718	0.3556

Main passerine lineages								
Z (means)	Clades	1	1*	2	3	4	5	6
4.22	P1. Passerida							
2.95	P1*. Passerida*	0.2589						
-0.92	P2. Muscicapida	0.0004	0.0042					
1.01	P3. Sylviida	0.0310	0.1133	0.0853				
1.48	P4. Corvides	0.0344	0.1352	0.0483	0.4225			
1.66	P5. Meliphagoidea	0.1284	0.2916	0.0321	0.2881	0.3401		
1.33	P6. Tyrannida	0.0635	0.1838	0.0544	0.3956	0.4631	0.3831	
0.00	P7. Furnariida	0.0053	0.0287	0.2609	0.2431	0.1755	0.1143	0.1739

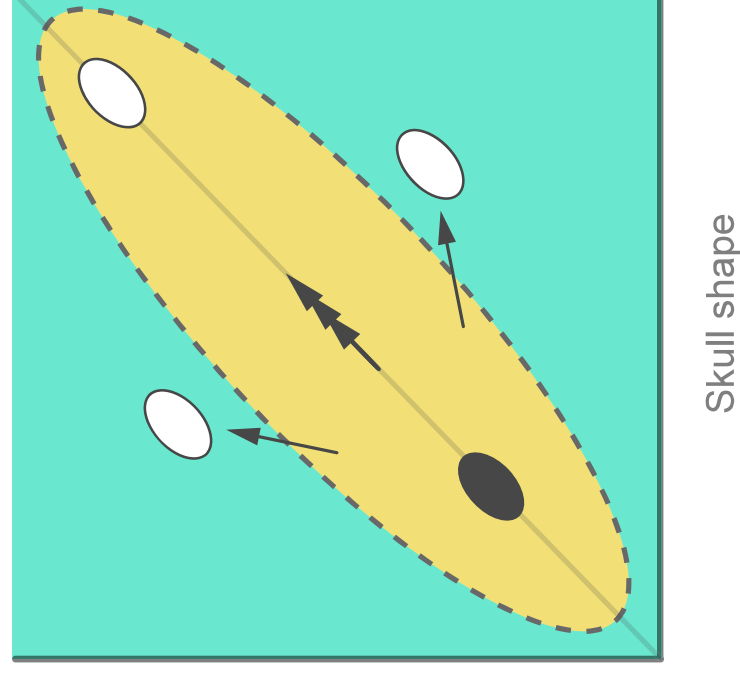
(a) Simulated phenotypic evolution



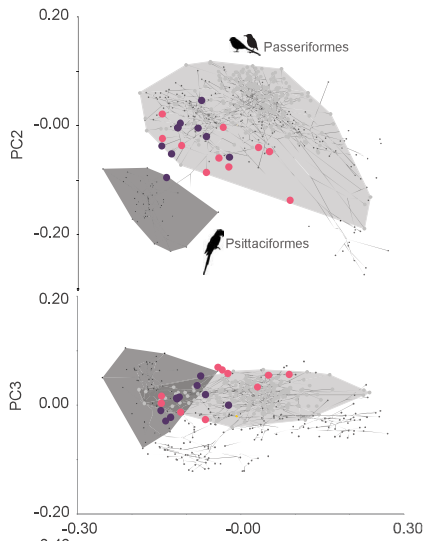
(b) Modular evolution



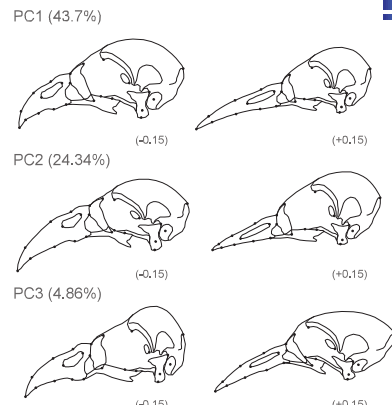
(c) Integrated evolution



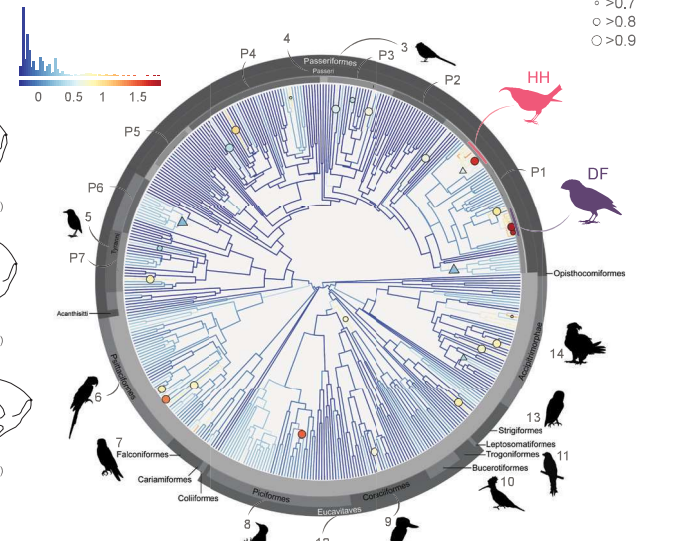
(a) *Phylomorphospaces*



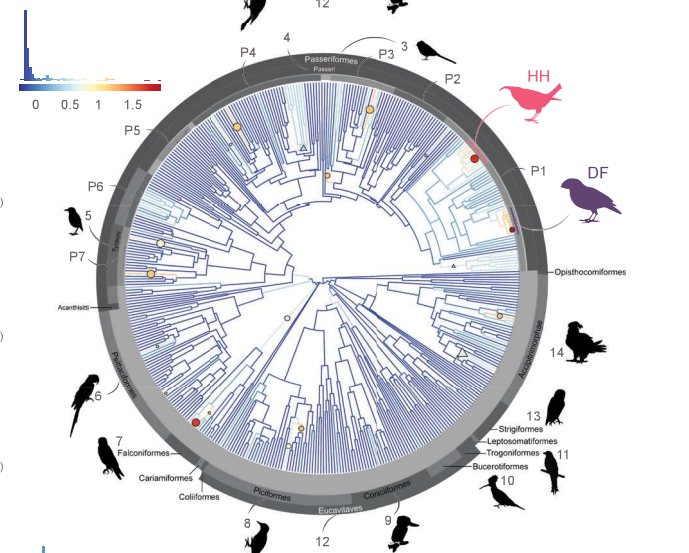
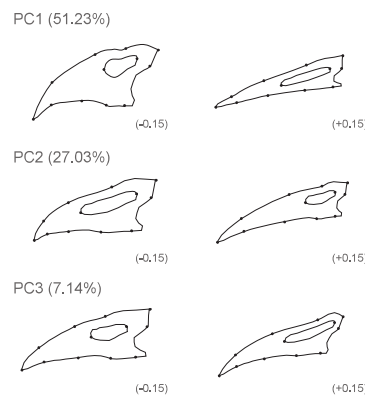
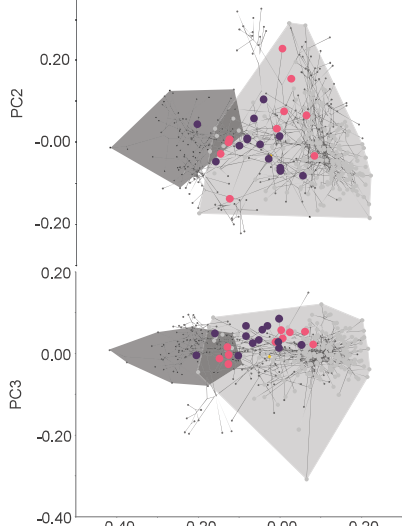
PC shape differences



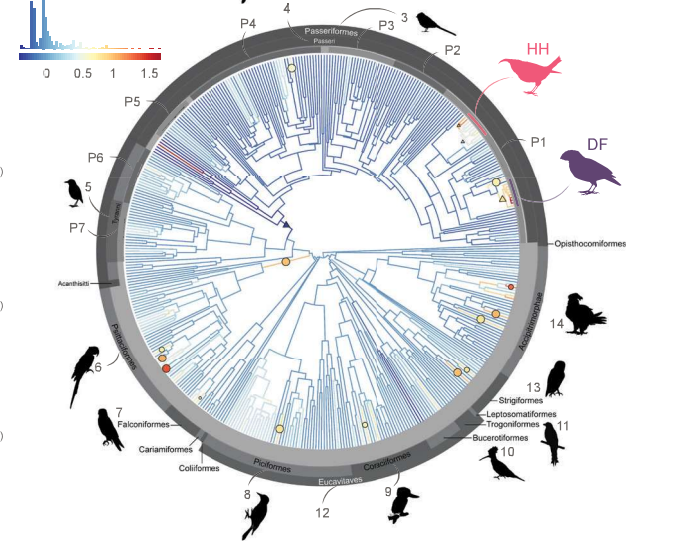
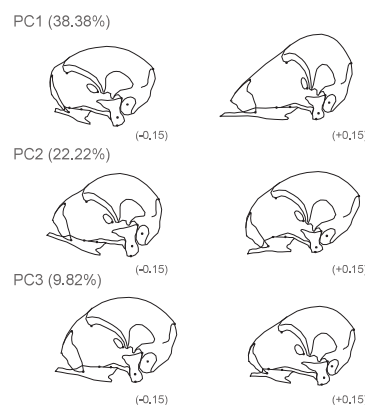
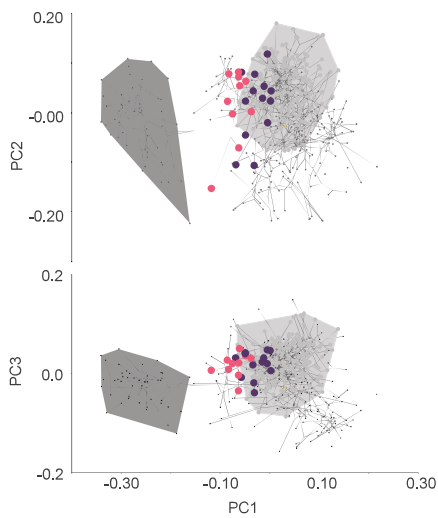
Frequency log relative rate



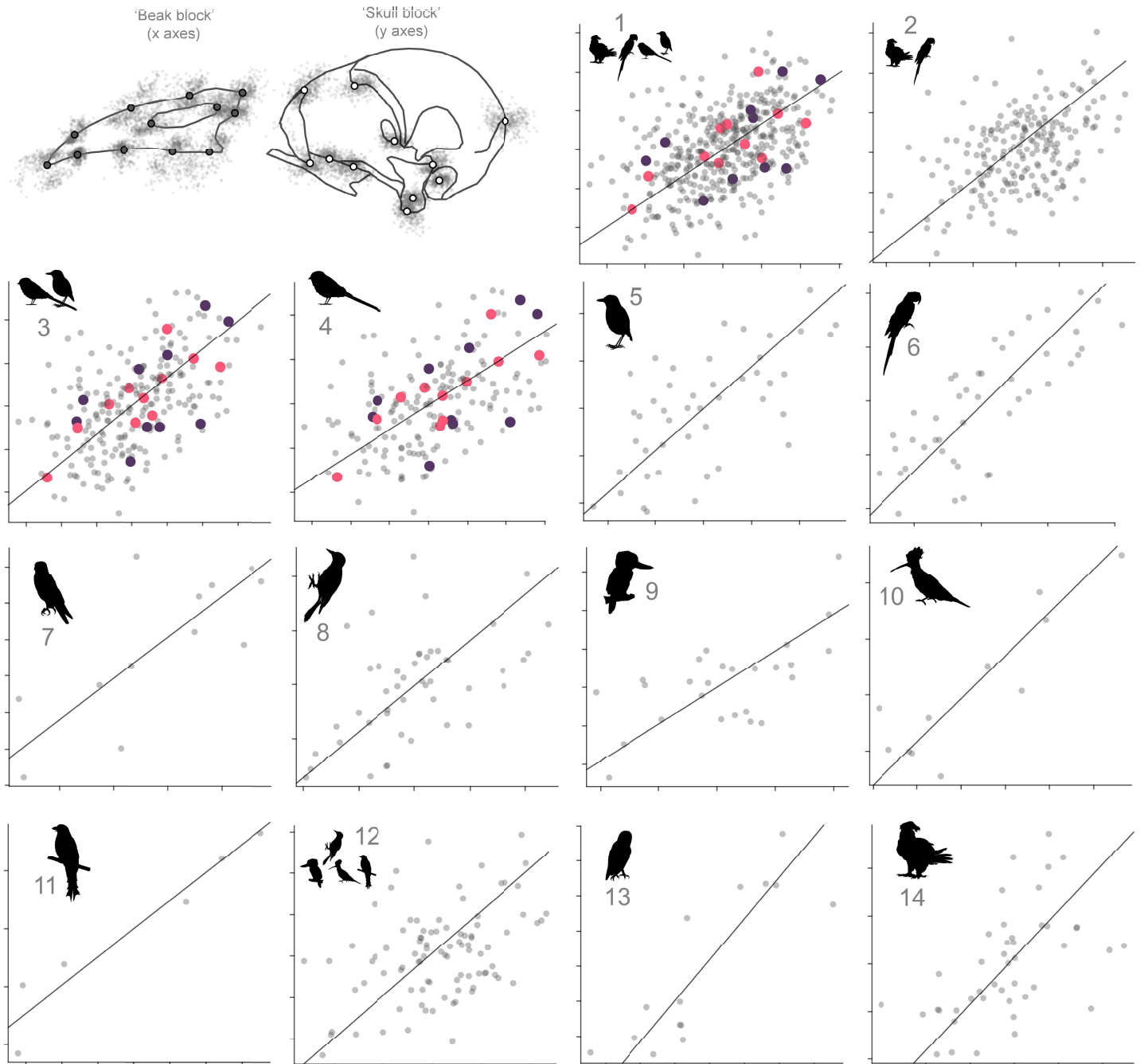
(b)



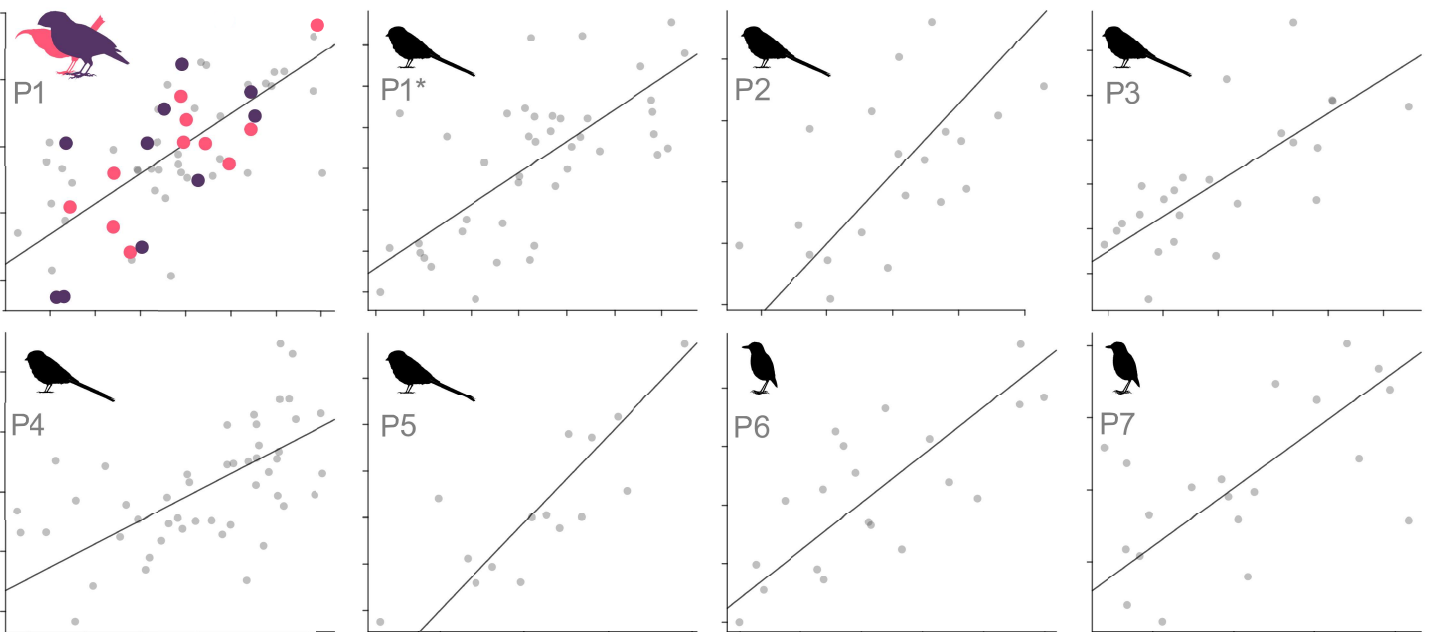
(c)



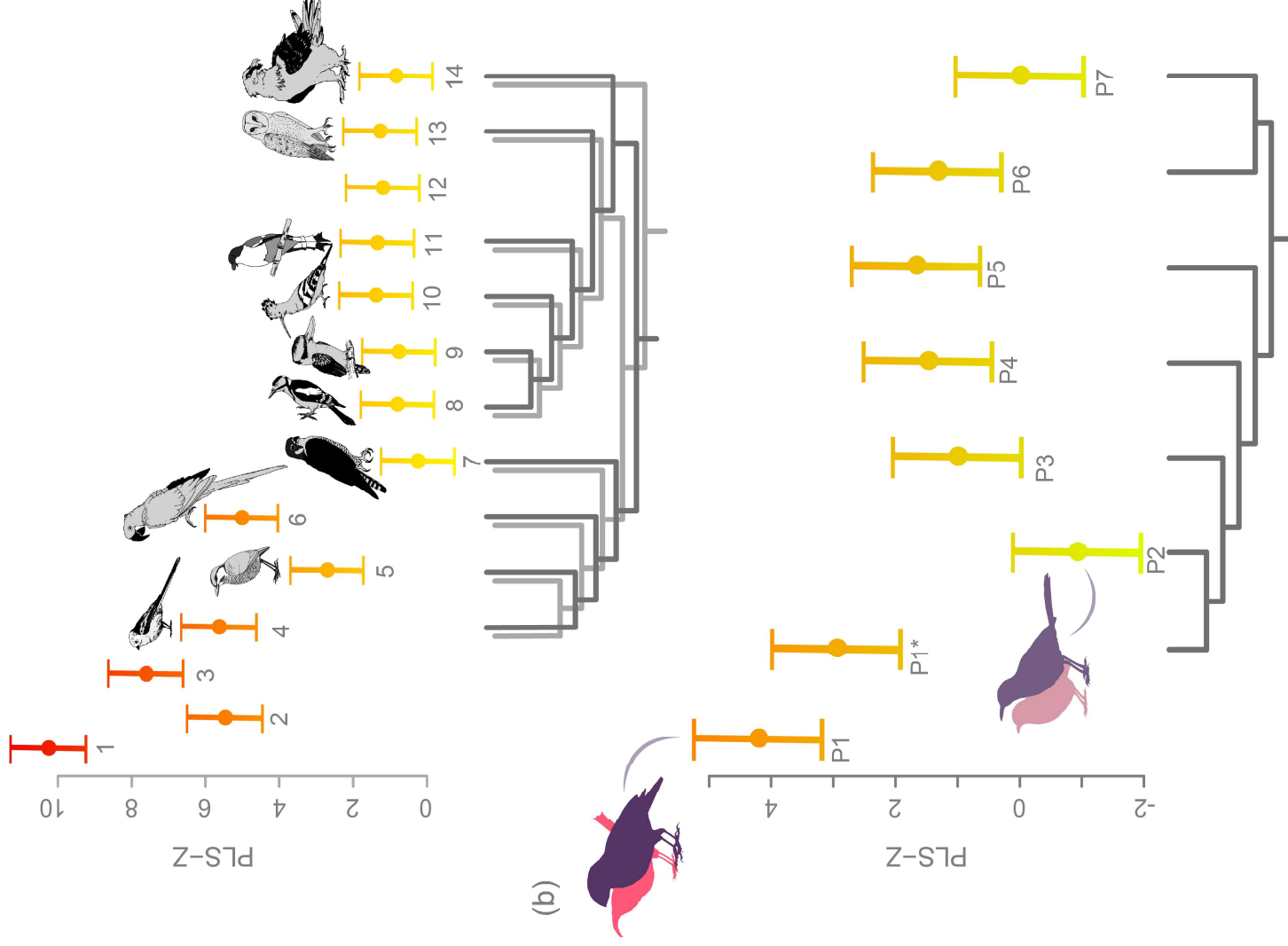
(a) *Phylogenetic Partial Least Squares*



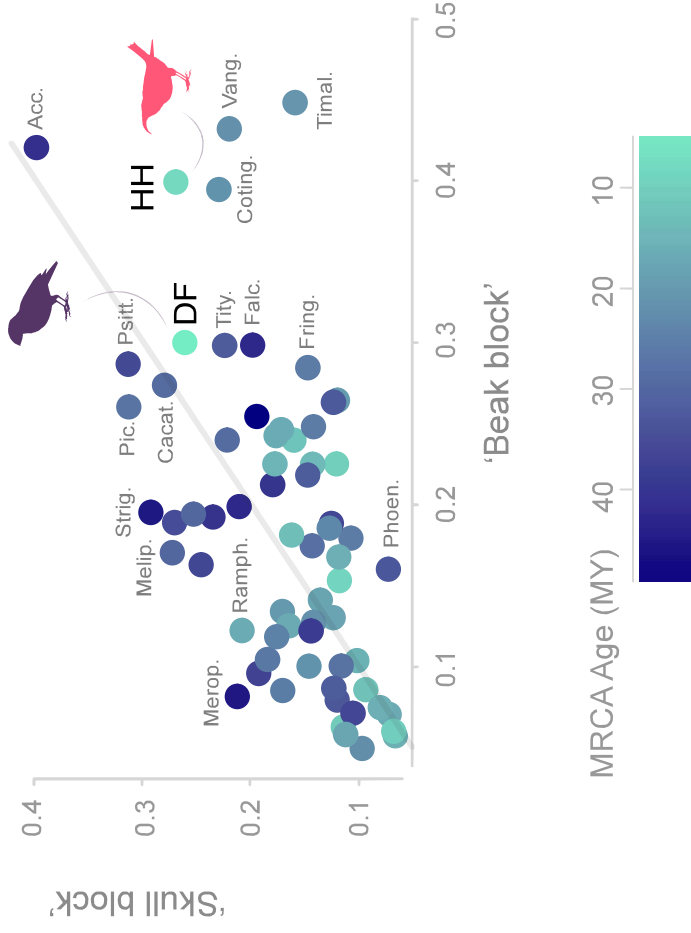
(b)



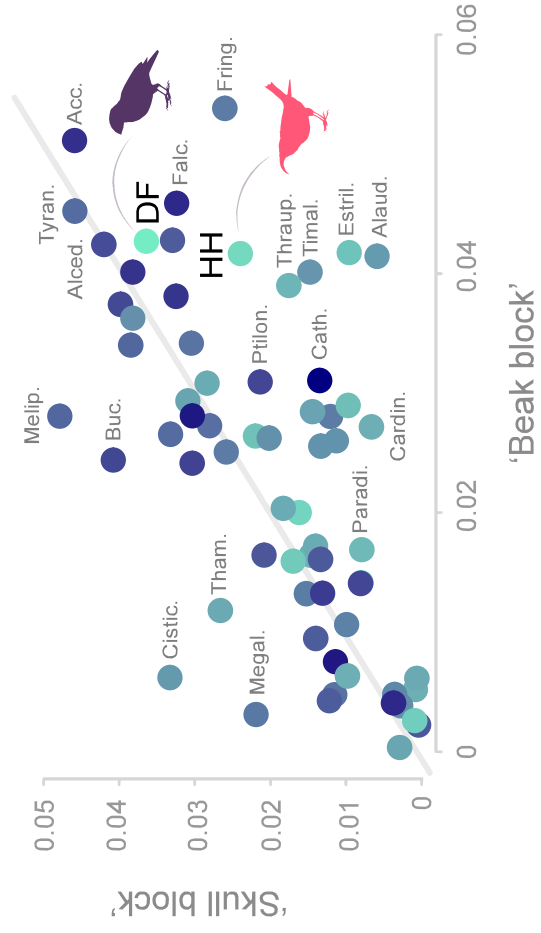
(a) Levels of integration

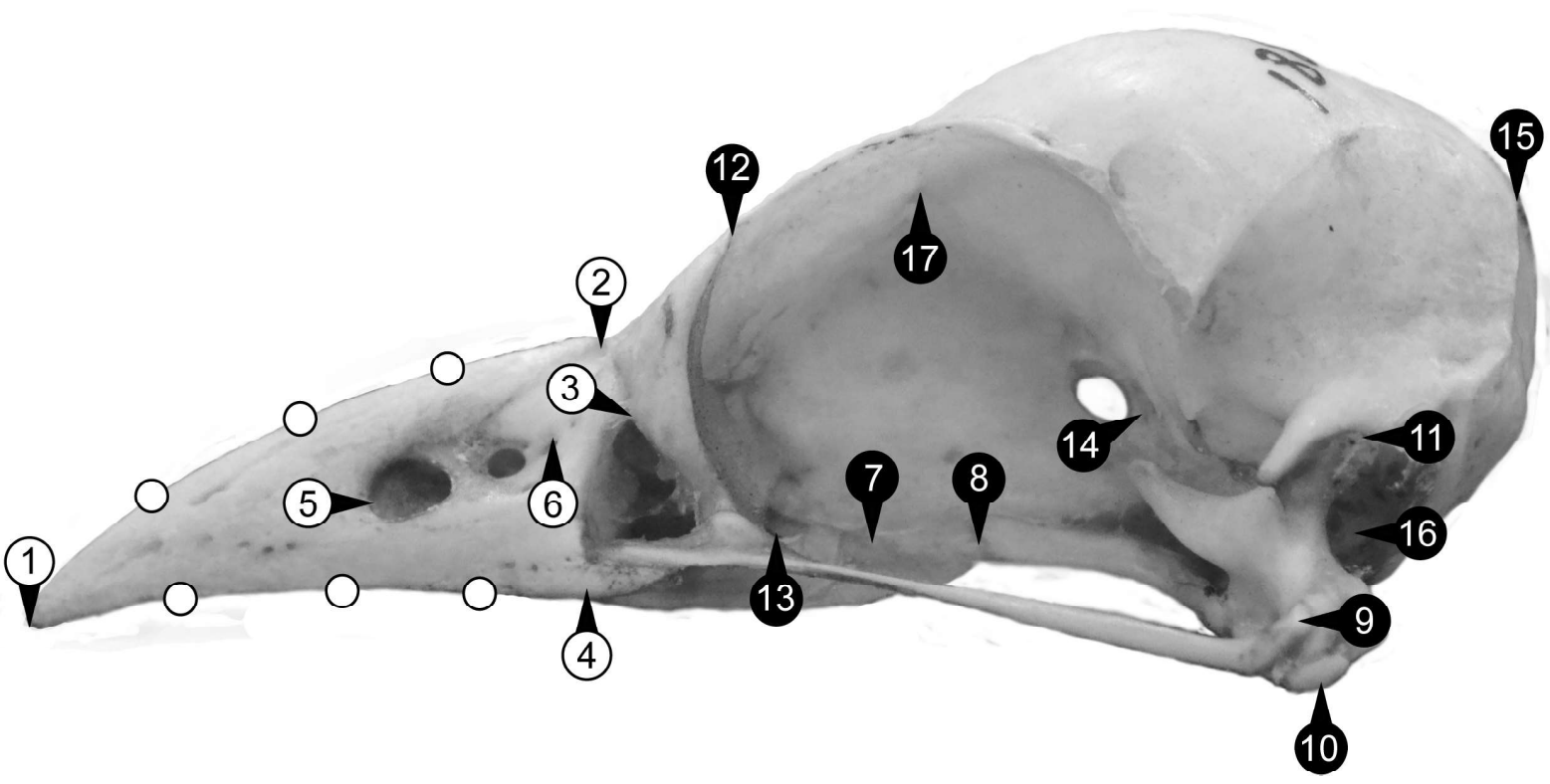


(c) Max. Proc. Distance within family



(d) Max. PLS1 Distance within family

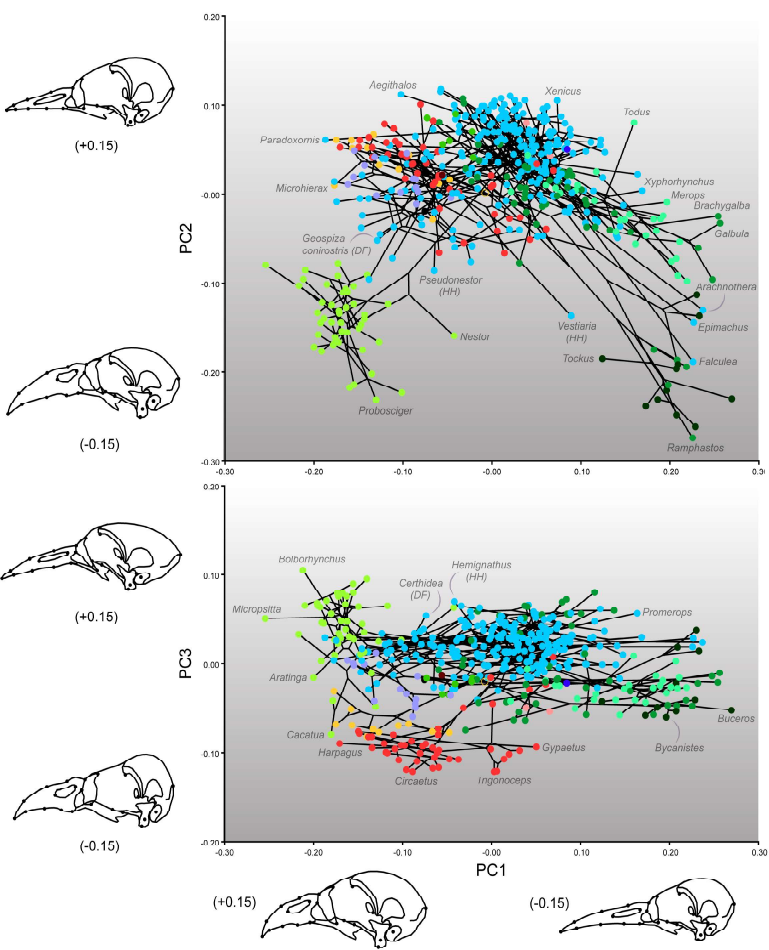




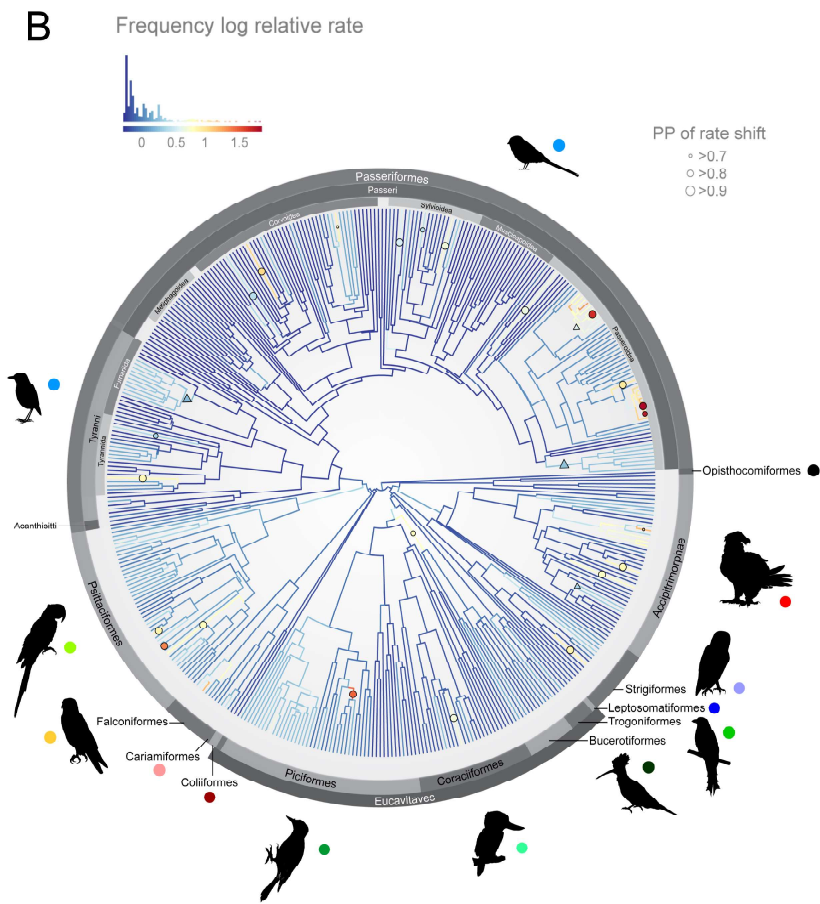
N	Block	Anatomical region	Description
1	Beak	Rostrum	Anterior tip of the premaxillary symphysis
2	Beak	Rostrum	Nasofrontal hinge
3	Beak	Rostrum	Ventrolateral end of the contact between nasal and lacrimal (or lacrimal-ectethmoid complex ^{**})
4	Beak	Rostrum	Antermost edge of antorbital fossa orthogonally projected to the ventral rim of the maxilla
5	Beak	Rostrum	Antermost point of external naris fossa
6	Beak	Rostrum	Posteriormost point of external naris fossa
7	Skull	Palate	Middle point of the medial contact between palatines
8	Skull	Palate	Middle point of the lateral contact of palatine and pterygoid
9	Skull	Quadrate	Medial condyle of quadrate
10	Skull	Quadrate	Contact of jugal bar and quadrate
11	Skull	Quadrate	Lateral contact of otic process of quadrate and squamosal
12	Skull	Lacrimal-ectethmoid	Posterolateral tip of lacrimal (or lacrimal-ectethmoid complex ^{**})
13	Skull	Lacrimal-ectethmoid	Posterolateral end of the contact between lacrimal (or lacrimal-ectethmoid complex ^{**}) and frontal
14	Skull	Neurocranium	Ventralmost point of the foramen of the optic nerve
15	Skull	Neurocranium	Intersection of <i>crista nuchalis transversus</i> and <i>crista nuchalis sagittalis</i>
16	Skull	Neurocranium	External ear (geometric centre of the auditory meatus)
17	Skull	Neurocranium	Foramen of the olfactory nerve (geometric centre)
18-21	Beak	Rostrum	Curve 1 of three semilandmarks along the beak culmen
21-24	Beak	Rostrum	Curve 2 of three semilandmarks along the right tomial ridge

^{**} term coined by Cracraft¹ to describe the coordinated evolution of both bones in modern birds which we used for the purposes of landmarking.

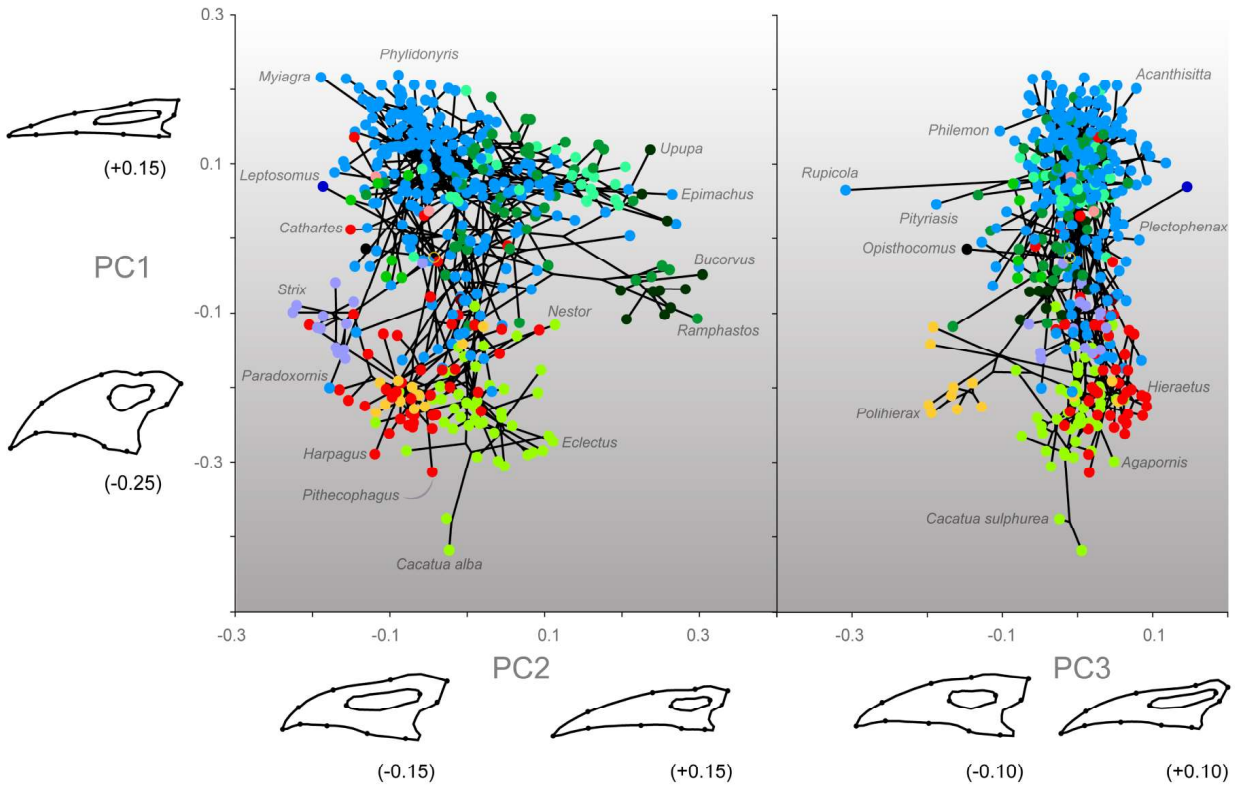
A



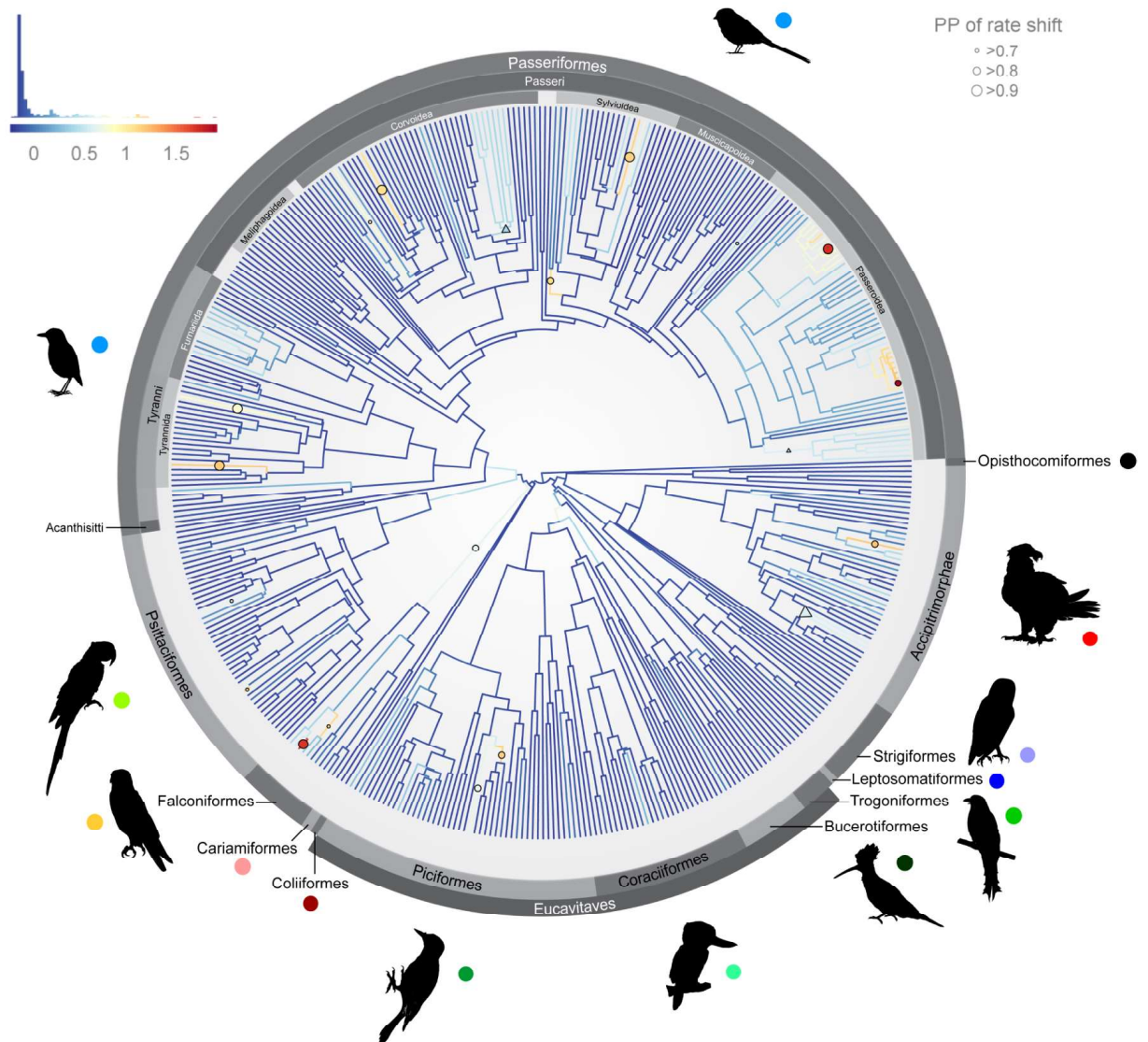
B

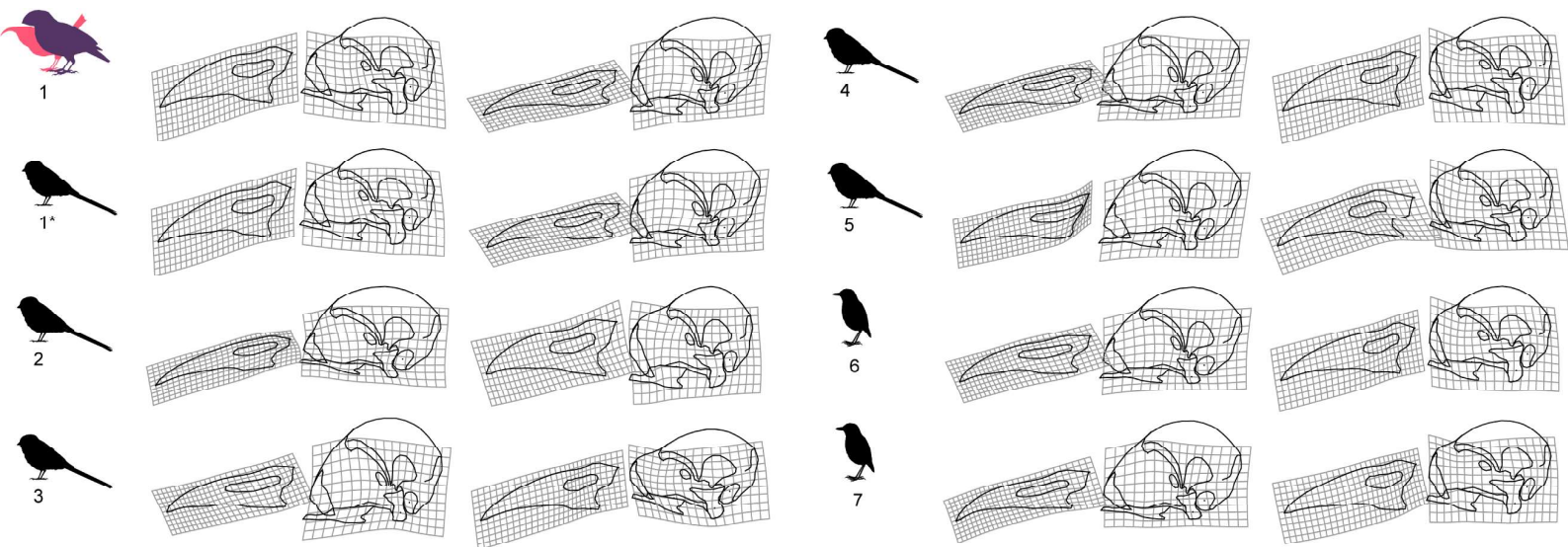
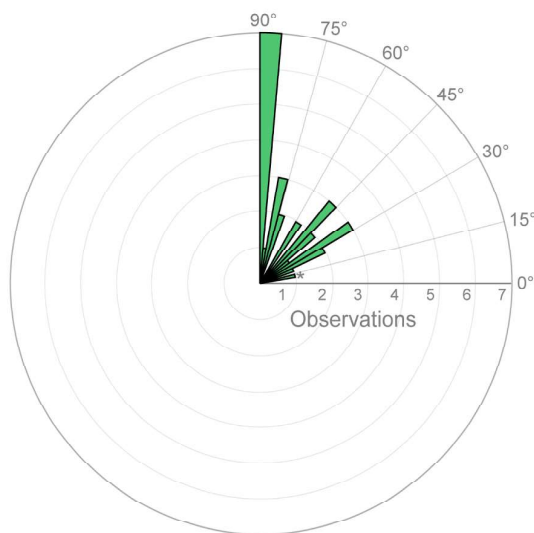
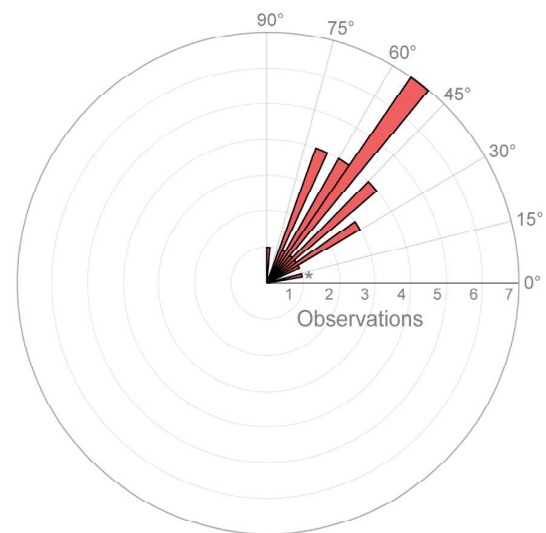


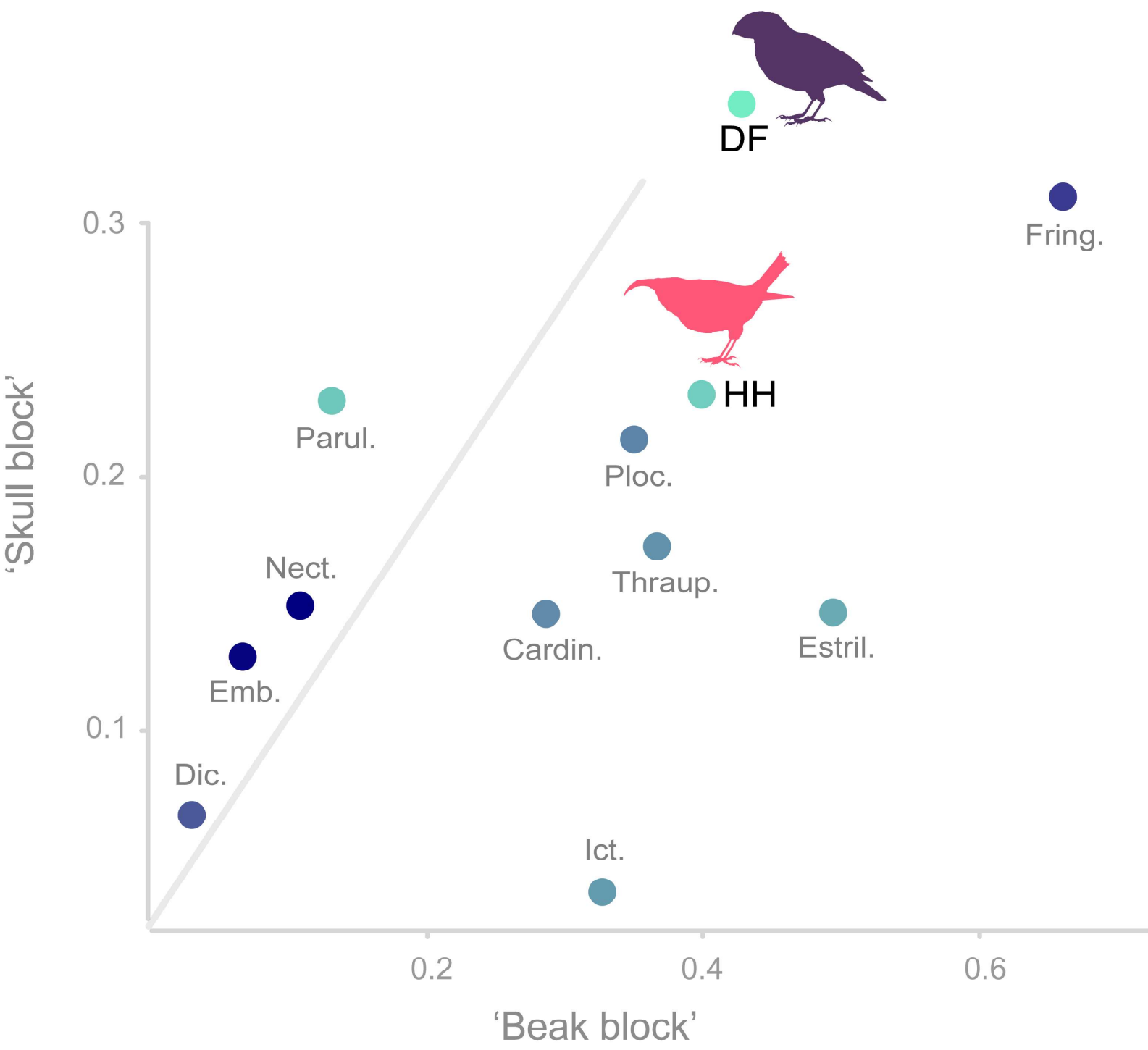
A



B



A**B****C**



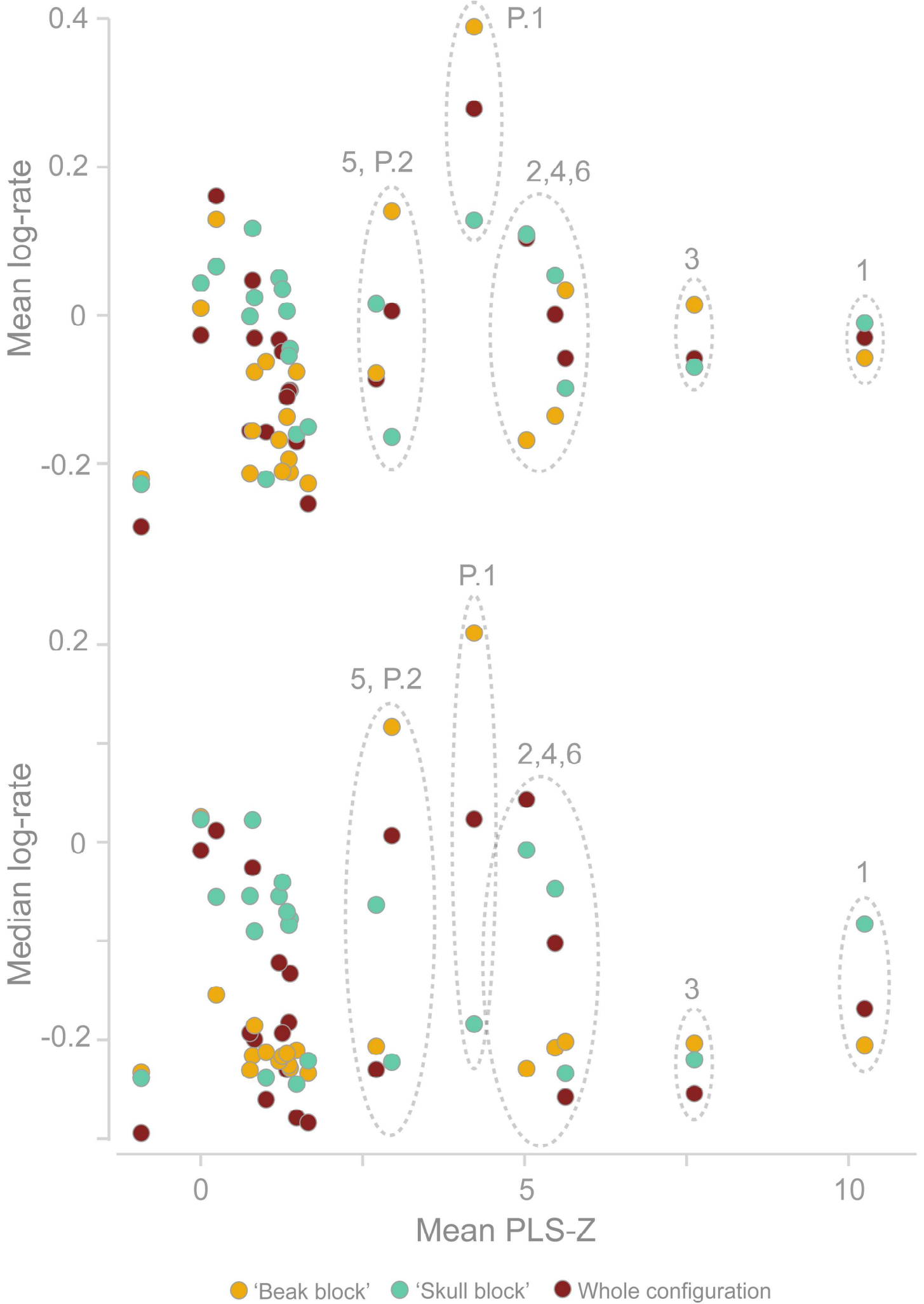
MRCA Age (MY)

30

20

10





● 'Beak block' ● 'Skull block' ● Whole configuration

Label	Family
Acanth.	Acanthisittidae
Acc.	Accipitridae
Alaud.	Alaudidae
Alced.	Alcedinidae
Brachyp.	Brachypteraciidae
Buc.	Bucerotidae
Bucc.	Bucconidae
Cacat.	Cacatuidae
Cardin.	Cardinalidae
Cath.	Cathartidae
Cistic.	Cisticolidae
Corac.	Coraciidae
Corv.	Corvidae
Coting.	Cotingidae
Crac.	Cracticidae
DF	Darwin's finches (Geospizinae, Thraupidae)
Dic.	Dicaedidae
Ember.	Emberizidae
Estril.	Estrildidae
Euryl.	Eurylaimidae
Falc.	Falconidae
Fring.	Fringillidae (excluding Hawaiian honeycreepers)
Furn.	Furnariidae
Galb.	Galbulidae
HH	Hawaiian honeycreepers (Drepanidinae, Fringillidae)
Hirun.	Hirundinidae
Ict.	Icteridae
Lyb.	Lybiidae
Megal.	Megalaimidae
Melip.	Meliphagidae
Merop.	Meropidae
Momot.	Momotidae
Nect.	Nectariniidae
Paradi.	Paradisaeidae
Parul.	Parulidae
Phoen.	Phoeniculidae
Pic.	Picidae
Pipr.	Pipridae
Pitt.	Pittidae
Ploc.	Ploceidae
Psitt.	Psittacidae
Ptilon.	Ptilonorhynchidae
Ramph.	Ramphastidae
Strig.	Strigidae
Sturn.	Sturnidae
Sylv.	Sylviidae
Tham.	Thamnophilidae
Thraup.	Thraupidae (excluding Darwin's finches)
Timal.	Timaliidae
Tity.	Tityridae
Trog.	Trogonidae
Tyran.	Tyrannidae
Vang.	Vangidae

Θ

BEAK	Passeriformes	Passeri	Tyranni
Passeroidea	27.57	23.17	44.37
Passeroidea*	31.35	28.70	43.59
Muscicapoidea	71.24	70.33	82.03
SKULL			
Passeroidea	30.98	27.51	41.32
Passeroidea*	33.69	29.63	43.42
Muscicapoidea	56.16	58.51	60.18